

# FFTArray: A Python Library for the Implementation of Discretized Multi-Dimensional Fourier Transforms

Stefan J. Seckmeyer<sup>1\*</sup>, Christian Struckmann<sup>1</sup>, Gabriel Müller<sup>1</sup>, Jan-Niclas Kirsten-Siemß<sup>1</sup> and Naceur Gaaloul<sup>1†</sup>

**1** Institut für Quantenoptik, Leibniz Universität Hannover, Welfengarten 1, D-30167, Hannover, Germany

\* [seckmeyer@iqo.uni-hannover.de](mailto:seckmeyer@iqo.uni-hannover.de) , † [gaaloul@iqo.uni-hannover.de](mailto:gaaloul@iqo.uni-hannover.de)

## Abstract

Partial differential equations describing the dynamics of physical systems rarely have closed-form solutions. Fourier spectral methods, which use Fast Fourier Transforms (FFTs) to approximate solutions, are a common approach to solving these equations. However, mapping Fourier integrals to discrete FFTs is not straightforward, as the selection of the grid as well as the coordinate-dependent phase and scaling factors require special care. Moreover, most software packages that deal with this step integrate it tightly into their full-stack implementations. Such an integrated design sacrifices generality, making it difficult to adapt to new coordinate systems, boundary conditions, or problem-specific requirements. To address these challenges, we present FFTArray, a Python library that automates the general discretization of Fourier transforms. Its purpose is to reduce the barriers to developing high-performance, maintainable code for pseudo-spectral Fourier methods. Its interface enables the direct translation of textbook equations and complex research problems into code, and its modular design scales naturally to multiple dimensions. This makes the definition of valid coordinate grids straightforward, while coordinate grid specific corrections are applied with minimal impact on computational performance. Built on the Python Array API Standard, FFTArray integrates seamlessly with array backends like NumPy, JAX and PyTorch and supports Graphics Processing Unit acceleration. The code is openly available at <https://github.com/QSTheory/fftarray> under Apache-2.0 license.

Copyright attribution to authors.

This work is a submission to SciPost Physics Codebases.

License information to appear upon publication.

Publication information to appear upon publication.

Received Date

Accepted Date

Published Date

## Contents

<b>1</b>	<b>Introduction</b>	<b>2</b>
<b>2</b>	<b>Discretization of the Fourier Transform</b>	<b>5</b>
2.1	A Discretized Fourier Transform	5
2.2	Implementation	6
2.3	Special Cases	7
2.3.1	Symmetric Frequency Space and $x_{\min} = 0$	8
2.3.2	Symmetric Position and Frequency Space	8

---

2.3.3 Convolution	9
2.3.4 Derivative	9
<b>3 The FFTArray Library</b>	<b>10</b>
3.1 The Dimension class: Defining Coordinate Grids	11
3.2 The Array class: Managing Values in Position and Frequency Space	13
3.2.1 Initialization	13
3.2.2 Fourier Transforms	14
3.2.3 Arithmetic Operations and Broadcasting	14
3.2.4 Indexing	15
3.3 Lazy Phase Factor Application	16
3.3.1 Addition and subtraction	17
3.3.2 Multiplication	18
3.3.3 Division	19
3.3.4 Absolute values	19
3.3.5 Showcase	20
3.4 Python Array API	20
3.4.1 JAX Tracing	22
<b>4 Examples</b>	<b>23</b>
4.1 Derivative	23
4.2 Solving the Schrödinger Equation	25
4.3 Bragg Diffraction of Matter Waves	27
4.3.1 Raman-Nath Regime	29
4.3.2 Bragg Regime	29
4.4 Finding the Ground State of the Two-Dimensional Isotropic Quantum Harmonic Oscillator	30
4.4.1 Single Precision Simulation (float32)	32
4.5 Finding a Two-Species Ground State in a Harmonic Trap	33
<b>5 Computational Performance Evaluation</b>	<b>35</b>
<b>6 Conclusion and Outlook</b>	<b>38</b>
<b>A Computation Speed as a Function of Time Steps and Function Samples</b>	<b>40</b>
A.1 Hardware Selection and System Details	40
A.2 Measurement Methodology	41
A.3 Scaling in the Number of Time Steps	41
A.4 Scaling in the Number of Samples and Shape of the Domain	43
<b>References</b>	<b>45</b>

---

## 1 Introduction

Many interesting and important physical systems are modeled by differential equations that often lack closed-form solutions. Fourier integrals often allow to formulate approximate solutions for these systems. Although performing these integrals analytically may still remain

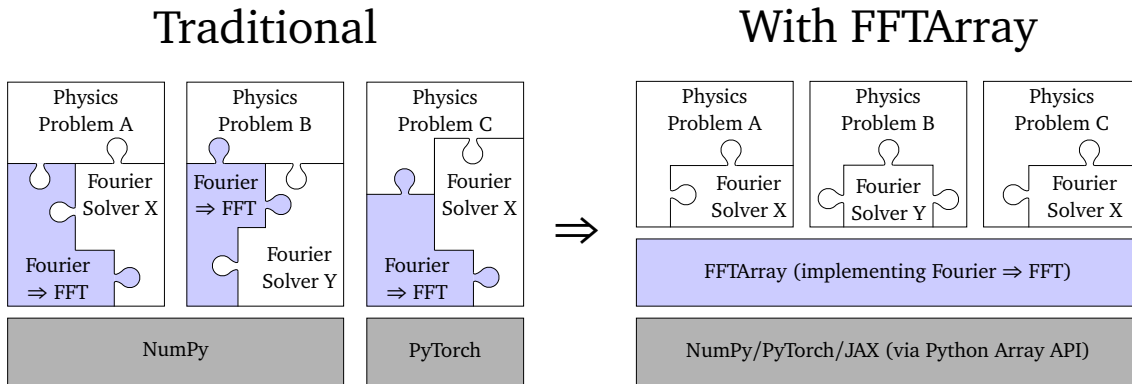


Figure 1: Conceptual overview of FFTArray’s role in scientific software architecture. Traditional software couples the definition of the physics problem, the Fourier-based differential equation solver and the discretization of Fourier transforms with Fast Fourier Transforms (FFTs) within a monolithic framework. These components interact with each other via problem-specific internal APIs, creating complex interdependent codebases. FFTArray decouples the implementation of discretized Fourier transforms from the solver and physics problem. This architectural simplification enables researchers to focus on core physics and solver logic without managing low-level FFT implementation details, resulting in more maintainable and reusable scientific code.

intractable, they can often be evaluated numerically by discretizing them and using Fast Fourier Transform (FFT) algorithms.

A prominent example is the Schrödinger equation, which governs the evolution of quantum mechanical systems ranging from single-particle dynamics to many-body phenomena. While exact solutions exist for idealized cases like box-shaped potentials and the quantum harmonic oscillator, most practical applications require numerical methods such as the split-step Fourier method [1, 2]. These numerical simulations allow the validation and improvement of analytical solutions as well as to go beyond our current understanding of complex physical systems.

Implementing a spectral Fourier solver for a particular problem can be split into three parts (fig. 1). At the input level, the user defines their system, representative of a concrete set of potentially time-dependent differential equations. In the case of the Schrödinger equation, this could be the initial state and the Hamiltonian of the system. The solver algorithm transforms these into a list of discrete steps to compute the current state of the system from its previous state. In the case of a spectral Fourier method, like a split-step Fourier solver, each of these steps contains multiple analytical Fourier integrals. These analytical expressions are discretized over a finite spatial volume with a finite sample spacing in order to evaluate them numerically. This involves the translation of the analytical Fourier integrals into Fast Fourier Transforms and must take into account the concrete system, the requirements of the solver as well as the coupling between the sample spacing in position and frequency space, described by the Sampling Theorem [3]. These three blocks are built on top of a general numerical array library, which in the case of Python are libraries like NumPy, JAX and PyTorch [4–6].

Existing implementations often entangle these logically distinct blocks - physical system definition, solver algorithms, and FFT-based discretization (fig. 1) - into application-specific frameworks [7–11]. This monolithic design creates three major limitations:

1. **Lack of generality:** Each implementation needs to focus on a specific subset of systems in order to keep complexity in check. Examples for such limitations are only simulating a single wave function or supporting only exactly two dimensions.

2. **Code duplication:** Due to the limited scope, one needs a new implementation for each significant change in the simulated system or used solver. Since each implementation might use special properties like symmetric grids to simplify their use of FFTs, the discretization of the analytic Fourier transforms into FFTs is re-derived and implemented.
3. **Code complexity:** Tight coupling between implementation shortcuts and special-case logic makes the code diverge significantly from its original mathematical formulation. Any modification to one part of the system risks breaking interconnected components, requiring coordinated updates and understanding across the entire codebase.

We have generally observed that managing these limitations presents a substantial challenge in the development of scientific simulations as systems grow in complexity. To conclude, integrating system definitions, solvers, and Fourier transforms into a monolithic program with narrow scope makes these programs challenging to maintain, reuse or adapt to new problems.

Here, we present the Python library FFTArray, which implements the numerical approximation of a Fourier transform with an FFT on arbitrarily placed multi-dimensional grids. Encapsulating this level cleanly allows numerical simulations to focus on the other two blocks and therefore be significantly simpler (as illustrated in fig. 1). The design and implementation of FFTArray focuses on three goals:

1. **From formulas to code:** Physicists can directly map analytical equations involving Fourier transforms to code without mixing discretization details with physics. This enables rapid prototyping of diverse physical models and solver strategies.
2. **State-of-the-art performance:** We achieve state-of-the-art performance on Graphics Processing Units (GPUs) when solving the Schrödinger equation via split-step algorithms for large quantum systems with more than  $10^9$  samples and more than  $10^4$  time steps.
3. **Seamless multidimensionality:** Dimensions are broadcast by name which enables a uniform API to seamlessly transition from single- to multi-dimensional systems.

FFTArray is a pure Python library built on top of the Python Array API standard in order to be accessible and maintainable in the future. This design ensures compatibility with the ubiquitous NumPy for smaller calculations in any environment, while also enabling GPU acceleration with JAX and PyTorch.

Despite its broad applicability, we note that FFTArray was developed in the context of simulating the atom-light interaction, dynamics and interferometry of ultracold atomic ensembles, particularly Bose-Einstein condensates (BECs) [12]. Thus, our examples and benchmarking focus on problems within this domain. The time evolution of these systems is determined by a nonlinear Schrödinger equation, referred to as the Gross-Pitaevskii equation (GPE) [13–15]. A concrete system can be simulated by solving this equation using the split-step method [16].

This paper is organized as follows: Section 2 introduces the mathematical framework for approximating the continuous Fourier transform on arbitrary coordinate grids using FFTs. It also highlights special cases of coordinate grid choices which are often chosen to simplify the use of the FFT. Section 3 outlines the rationale behind the design of the FFTArray library that allows near native performance and facilitate seamless interaction with various array libraries. In section 4, we present multiple application examples, ranging from performing a derivative to computing the quantum mechanical ground state of a coupled two-species mixture of Bose-Einstein condensates confined in a harmonic potential. We analyze the computational precision of FFTArray by comparing it with the analytical solution of the single-species isotropic quantum harmonic oscillator. Section 5 showcases the performance of FFTArray using NumPy and JAX on various central processing units (CPUs) and GPUs. This chapter also serves as a starting guide for developing efficient implementations of different solver algorithms based on FFTArray.

## 2 Discretization of the Fourier Transform

The Fourier transform converts an analytical function from its original domain  $x$  into its representation in the domain of the conjugate variable  $f$ , which we will refer to as the frequency domain [17]. The unit of  $f$  is given by the inverse of the unit of the variable  $x$  in the original domain  $[f] = [x]^{-1}$ . For a function  $g(x) : \mathbb{R} \rightarrow \mathbb{C}$  (including  $\mathbb{R} \rightarrow \mathbb{R}$ ), defined in the original domain, the Fourier transform  $\mathcal{F}$  returns a complex-valued function  $G(f) : \mathbb{R} \rightarrow \mathbb{C}$  in the frequency domain. This function gives the amplitudes and phases for all frequencies  $f$  which make up the original function. The inverse Fourier transform  $\widehat{\mathcal{F}}$  converts a function from the frequency domain back to the original domain:

$$\mathcal{F} : G(f) = \int_{-\infty}^{\infty} dx \ g(x) e^{-2\pi i f x}, \quad \forall f \in \mathbb{R}, \quad (1)$$

$$\widehat{\mathcal{F}} : g(x) = \int_{-\infty}^{\infty} df \ G(f) e^{2\pi i f x}, \quad \forall x \in \mathbb{R}. \quad (2)$$

The integrals in eqs. (1) and (2) must exist in order for the aforementioned definitions to be valid. For Schwartz functions  $\mathcal{S}(\mathbb{R})$ , the Fourier transformation defines a pointwise automorphism [17]. Its domain can be extended to distributions [18] and to  $L^2(\mathbb{R})$  functions by defining eq. (1) as the limit of the image of  $\mathcal{S}(\mathbb{R})$  functions that converge to a function in  $L^2(\mathbb{R})$  [19].

Note, that the above definition of the Fourier transform uses the linear frequency  $f$  as opposed to the circular frequency  $\omega = 2\pi f$ . The FFTArray library chooses the name "position space" for the original domain, which we will use from here on. This does not affect its applicability to Fourier transforms in time, where the position space is typically called "time domain".

For many functions it is not feasible to evaluate their Fourier transform analytically. Beyond trivial or well-known analytical functions it is often impractical to calculate the integral in eq. (1) analytically. Moreover, the sampled values of any measurement of a physical quantity or the output of a numerical algorithm do not have an analytical expression to perform the Fourier transform on.

### 2.1 A Discretized Fourier Transform

For the cases where analytically evaluating the Fourier transform is not feasible, one can construct a discretized analog of the Fourier transform. FFTArray focuses on a regular  $N$ -point grid with  $N$  equidistant samples  $x_n$  in position space and  $f_m$  in frequency space:

$$x_n := x_{\min} + n\Delta x, \quad n = 0, \dots, N-1, \quad (3)$$

$$f_m := f_{\min} + m\Delta f, \quad m = 0, \dots, N-1. \quad (4)$$

The sample spacings  $\Delta x, \Delta f > 0$  describe the distance between two samples and  $x_{\min}, f_{\min}$  are the smallest samples in position and frequency space, respectively.

One approach to discretize the function is to sample it in either position or frequency space without any prefiltering or postfiltering:

$$g_n := g(x_n), \quad (5)$$

$$G_m := G(f_m). \quad (6)$$

Using these definitions, we approximate the integrals from eq. (1) and eq. (2) as Riemann sums leading to a general discretized Fourier transform (gdFT and gdIFT):

$$G_m = \Delta x \sum_{n=0}^{N-1} g_n e^{-2\pi i f_m x_n} \quad (\text{gdFT}), \quad (7)$$

$$g_n = \Delta f \sum_{m=0}^{N-1} G_m e^{2\pi i f_m x_n} \quad (\text{gdIFT}). \quad (8)$$

Due to the discretized position space we can only distinguish frequencies within the range  $f_{\text{period}} = 1/(\Delta x)$  [20]. The same holds for the discrete frequency space which then results in the following coupling between position and frequency space<sup>1</sup>:

$$x_{\text{period}} := N \Delta x = \frac{1}{\Delta f}, \quad (9)$$

$$f_{\text{period}} := N \Delta f = \frac{1}{\Delta x}, \quad (10)$$

$$1 = N \Delta f \Delta x. \quad (11)$$

With eq. (11) the two transforms eq. (7) and eq. (8) are exact inverses to each other.

We emphasize that discretizing a continuous function and the Fourier transform has several non-trivial implications. We highlight the essentials in the context of this work and refer the reader to refs. [20–23] for extended discussions. The most central aspect of sampling is the Nyquist Shannon Sampling Theorem: If a function has finite bandwidth  $B$  (i.e. no spectral content beyond  $B$ ), sampling with  $\Delta x \leq 1/(2B)$  allows exact reconstruction [3]. Uniform sampling with  $\Delta x$  (and infinitely many samples) replicates the continuous spectrum with period  $1/(\Delta x)$ . If the bandwidth of the sampled function is larger than  $1/(2\Delta x)$ , these replicas of the function's frequency spectrum overlap. The contributions of any overlapping frequencies will appear as an additional amplitude and phase under a different "alias" frequency. Therefore, this process is also called aliasing [21]. Since most functions in practice are not strictly band-limited (e.g. a Gaussian wave packet has infinite extent in both position and frequency) care has to be taken to reduce aliasing. Depending on the application, this can be done for example by prefiltering or using a higher sampling rate. For a more exhaustive treatment of the different trade-offs in sampling continuous functions on an  $N$ -point grid, see for example refs. [23, 24].

The grid on which the g(I)DFT in eqs. (7) and (8) operate is periodic. In physics simulations this property can often be utilized as periodic boundary conditions [20]. On the other hand, an open domain can be approximated by zero-padding and/or using absorbing layers at the domain boundaries [22, 25].

Note, that these observations do not constrain the choice of the offsets  $x_{\text{min}}$  and  $f_{\text{min}}$ . In most band-limited cases the energy content of the function is centered at  $f = 0$  which makes centering the frequency space around zero the best choice. In other cases an asymmetric window can be beneficial since it is known that only specific frequencies appear in the sampled function. Examples for this are single-sideband modulated signals [3] or a quantum mechanical wavefunction describing a Gaussian wave packet with a non-zero velocity.

## 2.2 Implementation

The general discretized Fourier transform, eqs. (7) and (8), could be implemented directly and then used as a discrete analog to the continuous Fourier transform. But in practice, there

<sup>1</sup>Equation (11) is for  $f$  being in the unit of cycles. Without loss of generality it can be substituted by a variable in any unit. For example for an angular frequency  $k = 2\pi f$  eq. (11) would be  $2\pi = N \Delta k \Delta x$ .

are multiple optimizations possible to ensure the best computational performance. The most important optimization is to replace the naive sums by using Fast Fourier Transform (FFT) algorithms. The resulting expression can then often be simplified even further which is described in section 2.3.

From this point on, we extend the mathematical notation by functions which take an array as the input and return an array. The appearance of an index like  $n$  inside the argument of the function  $\text{dft}_m(g_n)$  marks  $\text{dft}$  as a function which takes an array in position space as an argument and returns an array in frequency space. The subscript  $n$  or  $m$  denotes the space of their result.

$$\text{dft}_m(g_n) \equiv \text{dft}_m(\{g_n\}_{n=0}^{N-1}) := \sum_{n=0}^{N-1} g_n e^{-2\pi i \frac{mn}{N}}, \quad (12)$$

$$\text{idft}_n(G_m) \equiv \text{idft}_n(\{G_m\}_{m=0}^{N-1}) := \frac{1}{N} \sum_{m=0}^{N-1} G_m e^{+2\pi i \frac{mn}{N}}. \quad (13)$$

The DFT and inverse DFT have multiple conventions for phase and scaling factors. The above definitions follow NumPy [4], the standard library of scientific computing in Python. Evaluating these sums naively has a computational time complexity of  $\mathcal{O}(N^2)$ . They can be computed more efficiently with Fast Fourier transform (FFT) algorithms in  $\mathcal{O}(N \log N)$  time.

To be able to calculate eqs. (7) and (8) in  $\mathcal{O}(N \log N)$  steps we decompose them into separate phase factors and express them in terms of the  $\text{fft}$  and  $\text{ifft}$ :

$$(\text{gdFT}) \quad G_m = \Delta x \sum_{n=0}^{N-1} g_n e^{-2\pi i (f_{\min} + m\Delta f)(x_{\min} + n\Delta x)} \quad (14)$$

$$= \Delta x e^{-2\pi i x_{\min} m\Delta f} e^{-2\pi i x_{\min} f_{\min}} \sum_{n=0}^{N-1} g_n \underbrace{e^{-2\pi i m\Delta f n\Delta x}}_{e^{-2\pi i \frac{mn}{N}}} e^{-2\pi i f_{\min} n\Delta x} \quad (15)$$

$$= \Delta x e^{-2\pi i x_{\min} m\Delta f} e^{-2\pi i x_{\min} f_{\min}} \text{fft}_m(g_n e^{-2\pi i f_{\min} n\Delta x}), \quad (16)$$

$$(\text{gdIFT}) \quad g_n = \Delta f \sum_{m=0}^{N-1} G_m e^{2\pi i (f_{\min} + m\Delta f)(x_{\min} + n\Delta x)} \quad (17)$$

$$= \Delta f e^{+2\pi i f_{\min} n\Delta x} \sum_{m=0}^{N-1} G_m \underbrace{e^{+2\pi i m\Delta f n\Delta x}}_{e^{+2\pi i \frac{mn}{N}}} e^{+2\pi i x_{\min} m\Delta f} e^{+2\pi i x_{\min} f_{\min}} \quad (18)$$

$$= e^{+2\pi i f_{\min} n\Delta x} \Delta f N \text{ ifft}_m(G_m e^{+2\pi i x_{\min} m\Delta f} e^{+2\pi i x_{\min} f_{\min}}) \\ = e^{+2\pi i f_{\min} n\Delta x} \text{ ifft}_m(G_m e^{+2\pi i x_{\min} m\Delta f} e^{+2\pi i x_{\min} f_{\min}} / \Delta x). \quad (19)$$

Identical colors highlight exponentials with opposite signs for the forward and backward transforms. The grouping of the factors and the use of eq. (11) in the last step makes the forward and backward transform symmetric which becomes important in section 3.3. All remaining phase factors only depend on at most one of the indices and can therefore be applied to the values before or after the transform in linear time  $\mathcal{O}(N)$ . Therefore the complete algorithm has a runtime complexity of  $\mathcal{O}(N \log N)$ .

## 2.3 Special Cases

In many common applications it is possible to remove some of the additional phase terms while still getting correct results for that use case. In this section we discuss some of these special

cases and the simplifications they allow. This then also shows the use-cases for the common helper functions for FFTs `fftshift`, `ifftshift` and `fftfreq` as defined in NumPy [26]. These functions implement special cases of the general phase factors which are used by FFT-Array. Therefore when using the gd(I)FT via FFTArray these functions are not needed. To properly make the connection between FFTArray and many existing tutorials and implementations, we show in this section how the gd(I)FT can be rewritten in terms of these functions in some special cases of coordinate grids.

The factors  $\exp(\pm 2\pi i x_{\min} m\Delta f)$  and  $\exp(\pm 2\pi i f_{\min} n\Delta x)$  are special cases of shifting a function. Multiplying a function with the factor  $\exp(+2\pi i f_{\min} x)$  in position space or  $\exp(-2\pi i x_{\min} f)$  in frequency space shifts that function in the other space by  $f_{\min}$  or  $x_{\min}$  respectively. Since eqs. (16) and (19) operate on periodic functions, these shifts are cyclic. Any part of the function that is shifted out of the position or frequency window on one side directly reappears on the other side. If  $x_{\min}$  or  $f_{\min}$  are integer multiples of  $\Delta x$  or  $\Delta f$ , their shifts can be replaced by cyclically shifting the values in the array. Any values which move beyond the end of the array are moved back to the beginning. The functions `fftshift`, `ifftshift` implement such cyclic shifts for half the length of the domain.

### 2.3.1 Symmetric Frequency Space and $x_{\min} = 0$

Sampling a real-valued function is a common special case that can be found in many tutorials. Starting the sampling at  $x_{\min} = 0$  is often a natural choice like for example in a time series. With  $x_{\min} = 0$ , the gd(I)FT simplifies to:

$$\begin{aligned} \text{(gdFT with } x_{\min} = 0) \quad G_m &= \Delta x \text{ fft}_m(g_n e^{-2\pi i f_{\min} n\Delta x}), \\ \text{(gdIFT with } x_{\min} = 0) \quad g_n &= e^{+2\pi i f_{\min} n\Delta x} \text{ ifft}_m(G_m/\Delta x). \end{aligned}$$

The frequency space representation of such a function is conjugate symmetric ( $G(f) = \overline{G(-f)}$ ) and therefore frequency space must be chosen symmetrically:

$$f_{\min}^{\text{sym}} = -\text{floor}(0.5N)\Delta f. \quad (20)$$

Since  $f_{\min}^{\text{sym}}$  is an integer multiple of  $\Delta f$ , the exponential  $e^{\pm 2\pi i f_{\min} n\Delta x}$  can be replaced by a simple shift of the values. These shifts by  $f_{\min}^{\text{sym}}$  are implemented in `fftshift` and its inverse `ifftshift`. Replacing the remaining phase factors with these functions reduces the gd(I)FT to the more commonly known form:

$$\begin{aligned} \text{(gdFT with } x_{\min} = 0, f_{\min} = f_{\min}^{\text{sym}}) \quad G_m &= \Delta x \text{ fftshift}_m(\text{fft}_m(g_n)), \\ \text{(gdIFT with } x_{\min} = 0, f_{\min} = f_{\min}^{\text{sym}}) \quad g_n &= \text{ifft}_m(\text{ifftshift}_m(G_m/\Delta x)). \end{aligned}$$

### 2.3.2 Symmetric Position and Frequency Space

The special case of a position and frequency space, both symmetric around zero with zero being explicitly sampled allows to replace all phase factors with `fftshift` and `ifftshift` as well. A subtlety of this case is that  $x = 0$  and  $f = 0$  need to be sampled explicitly regardless of whether  $N$  is even or odd, analogous to the symmetric frequency space case:

$$x_{\min}^{\text{sym}} = -\text{floor}(0.5N)\Delta x, \quad (21)$$

$$f_{\min}^{\text{sym}} = -\text{floor}(0.5N)\Delta f. \quad (22)$$

Note that the samples in both position and frequency space with these choices for  $x_{\min}$  and  $f_{\min}$  are not actually symmetric for even  $N$ . Recalling eq. (3) and eq. (4) shows that there is

one more negative than positive coordinate value. With the coordinates properly chosen as in eqs. (21) and (22) the gd(I)FT can be written as:

$$\begin{aligned} (\text{gdFT with } x_{\min} = x_{\min}^{\text{sym}}, f_{\min} = f_{\min}^{\text{sym}}) \quad G_m &= \Delta x \text{ fftshift}_m(\text{fft}_m(\text{ifftshift}_n(g_n))), \\ (\text{gdIFT with } x_{\min} = x_{\min}^{\text{sym}}, f_{\min} = f_{\min}^{\text{sym}}) \quad g_n &= \text{fftshift}_n(\text{ifft}_m(\text{ifftshift}_m(G_m/\Delta x))). \end{aligned}$$

### 2.3.3 Convolution

Another common case where parts of the gd(I)FT can be simplified is the convolution. The convolution has many different applications ranging from image processing over statistics to physics [21, 27, 28]. It can be expressed with (inverse) Fourier transforms via the convolution theorem:

$$g(x) * h(x) = \int_{-\infty}^{\infty} g(\tau)h(x - \tau) d\tau \quad (23)$$

$$= \widehat{\mathcal{F}}\{\mathcal{F}[g(x)] \mathcal{F}[h(x)]\}. \quad (24)$$

This enables its computation on discretized data in  $\mathcal{O}(N \log N)$  via the FFT. In the general case of arbitrary  $x_{\min}$  and  $f_{\min}$ , one set of the phase and scale factors in frequency space cancels out. However, another set remains because there are two gdFTs and only one gdIFT:

$$\begin{aligned} g_n * h_n &= \text{gdIFT}_n(\text{gdFT}_m(g_n) \text{gdFT}_m(h_n)) \\ &= e^{+2\pi i f_{\min} n \Delta x} \text{ifft}_m[ \\ &\quad \Delta x e^{-2\pi i x_{\min} m \Delta f} e^{-2\pi i x_{\min} f_{\min}} \text{fft}_m(h_n e^{-2\pi i f_{\min} n \Delta x}) \\ &\quad \Delta x e^{-2\pi i x_{\min} m \Delta f} e^{-2\pi i x_{\min} f_{\min}} \text{fft}_m(g_n e^{-2\pi i f_{\min} n \Delta x}) \\ &\quad e^{+2\pi i x_{\min} m \Delta f} e^{+2\pi i x_{\min} f_{\min}} \frac{1}{\Delta x} \\ &\quad ] \\ &= e^{+2\pi i f_{\min} n \Delta x} \text{ifft}_m( \\ &\quad \Delta x e^{-2\pi i x_{\min} m \Delta f} e^{-2\pi i x_{\min} f_{\min}} \text{fft}_m(g_n e^{-2\pi i f_{\min} n \Delta x}) \text{fft}_m(h_n e^{-2\pi i f_{\min} n \Delta x}) \\ &\quad ). \end{aligned}$$

In this case it is important to actually apply these remaining phase and scale factors correctly to get the expected result. For special cases of  $x_{\min}$  and  $f_{\min}$  these shifts can again be replaced by `fftshift`, `ifftshift` or the identity as shown in the other examples.

### 2.3.4 Derivative

Computing a derivative via the Fourier transform can be viewed as a special case of the convolution. In this case one of the convolved functions can be constructed directly in frequency space (for details cf. section 4.1):

$$\frac{d}{dx} g(x) = \widehat{\mathcal{F}}\{(2\pi i f) \mathcal{F}\{g(x)\}\}. \quad (25)$$

Discretizing this using the gd(I)FT with  $x_{\min} = 0$  removes most phase factors:

$$\frac{d}{dx} g_n = \text{gdIFT}_n(2\pi i (f_{\min} + m \Delta f) \text{gdFT}_m(g_n)) \quad (26)$$

$$= e^{+2\pi i f_{\min} n \Delta x} \text{ifft}_m(2\pi i (f_{\min} + m \Delta f) \text{fft}_m(g_n e^{-2\pi i f_{\min} n \Delta x})). \quad (27)$$

Choosing a frequency space symmetric around zero with  $f_{\min} = f_{\min}^{\text{sym}}$  allows to replace the remaining phase factors with `fftshift`. The result can be simplified to only require `fftshift` once. Since it is then only needed in the construction of the frequency space coordinates, many FFT libraries provide a helper function called `fftfreq` to construct them directly:

$$\begin{aligned}
 & \text{Set } f_{\min} := f_{\min}^{\text{sym}} \\
 & \Rightarrow \frac{d}{dx} g_n = e^{+2\pi i f_{\min}^{\text{sym}} n \Delta x} \text{ ifft}_m( \\
 & \quad 2\pi i (f_{\min}^{\text{sym}} + m \Delta f) \text{ fft}_m(g_n e^{-2\pi i f_{\min}^{\text{sym}} n \Delta x}) \\
 & \quad ) \\
 & = \text{ifft}_m(\text{ifftshift}_m( \\
 & \quad 2\pi i (f_{\min}^{\text{sym}} + m \Delta f) \text{ fftshift}_m(\text{fft}_m(g_n)) \\
 & \quad )) \\
 & = \text{ifft}_m( \\
 & \quad \text{ifftshift}_m(2\pi i (f_{\min}^{\text{sym}} + m \Delta f)) \\
 & \quad \text{ifftshift}_m(\text{fftshift}_m(\text{fft}_m(g_n))) \\
 & \quad ) \\
 & = \text{ifft}_m( \\
 & \quad 2\pi i \text{ ifftshift}_m(f_{\min}^{\text{sym}} + m \Delta f) \text{ fft}_m(g_n) \\
 & \quad ) \\
 & = \text{ifft}_m( \\
 & \quad 2\pi i \text{ fftfreq}_m(N, \Delta x) \text{ fft}_m(g_n) \\
 & \quad ). 
 \end{aligned}$$

As shown in the examples above, the specific possible optimizations differ a lot for different use cases.

### 3 The FFTArray Library

FFTArray enables an easy to use general discretized Fourier transform while comprehensively addressing all special cases outlined in section 2.3 by implementing the general discretized Fourier transforms (gd(I)FT) in eqs. (16) and (19). By providing a modular toolkit for seamlessly and efficiently manipulating discretized functions in their position and frequency space representations it replaces the handling of grid-specific complexities with the common FFT library helpers `fftshift`, `ifftshift` and `fftfreq`. In contrast to the few discrete shifts supported by these methods FFTArray supports arbitrarily shifted coordinate grids.

Two core classes, `Dimension` and `Array`, automatically track coordinate grids and apply FFTs and phase factors where necessary. The `Dimension` class (section 3.1) encapsulates the position and frequency grids of a single dimension. The parameters of both domains can be initialized in the way most convenient for the current problem via a constraint solver. It ensures that the constraint in eq. (11) is always fulfilled and  $N$  is even or a power of two. The `Array` class (section 3.2) manages multi-dimensional sampled functions, their Fourier transforms and general mathematical operations. It stores the sample values and `Dimension` objects, while tracking for each axis whether it is in position space ( $g_n$ ) or frequency space ( $G_m$ , as formalized in section 2). Transformations between domains are executed implicitly by

setting the desired space for each dimension and automatically handling the required parts of the gd(I)FT. During arithmetic operations involving `Array` instances dimensions are broadcast based on their names. Both classes are immutable and all operations on an `Array` create a new array which reuses the values of one of its inputs if possible.

To minimize computational overhead, unnecessary scale and phase factors are automatically omitted in a user-controllable and predictable manner as detailed in section 3.3. By leveraging the Python Array API standard [29] (cf. section 3.4), `FFTArray` ensures portability and allows for higher performance by utilizing hardware accelerators like GPUs.

Smaller code examples are given in a Read-eval-print-loop (REPL) style. Python expressions and code lines are preceded with a `>>>` and the result of that line is printed below<sup>2</sup>. Variables are prefixed with `np_` for NumPy Arrays, `dim_` for `fa.Dimension` objects and `arr_` for `fa.Array` objects. The import below is used in all examples in this chapter.

```
1  >>> import fftarray as fa
```

Additionally variables defined in earlier snippets are still available for reuse in later snippets.

### 3.1 The Dimension class: Defining Coordinate Grids

`FFTArray` automatically handles arbitrary coordinate grids and ensures their validity such that the user can simply choose the grid best suited to the problem. This design avoids mistakes when defining grids which must fulfill the dependencies given in table 1. Additionally it standardizes which variables are used to uniquely define the grid coordinates.

The `Dimension` class represents the coordinate grids for one dimension in position and frequency space. It stores the name of the dimension and the numerical parameters  $N$ ,  $\Delta x$ ,  $x_{\min}$ , and  $f_{\min}$ .  $\Delta f$  can be obtained via eq. (11) from a given  $N$  and  $\Delta x$ . To initialize a `Dimension` from a set of parameters which does not consist of exactly  $N$ ,  $\Delta x$ ,  $x_{\min}$ , and  $f_{\min}$ , the system of equations in table 1 must be solved. For example, given the grid spacings  $\Delta x$  and  $\Delta f$  one would have to solve eq. (11) for  $N$ . However, this solution for  $N$  might not be an integer, which means, that either  $\Delta f$  or  $\Delta x$  or both parameters need to be adapted. Moreover, specific applications may have their own particular set of constraints on the definition on the grids, e.g., the position grid may need to be symmetric around a center point  $x_{\text{middle}}$  or the frequency grid may need to accommodate a function with an upper band limit of  $f_{\max}$ .

`FFTArray` allows to use any combination of grid parameters to initialize a `Dimension`. Internally, `FFTArray` uses the `z3` solver [30] for solving the constraints in table 1. This way, the user is not required to do so by hand. For example, a grid with  $N = 2048$ ,  $x_{\min} = -100$ ,  $x_{\max} = 50$  that is centered in frequency space can be initialized with<sup>3</sup>:

```
1  >>> fa.dim_from_constraints("x", n=2048, pos_min=-100., pos_max=50.,
2  ↵  freq_middle=0.)
2  Dimension(name='x', n=2048, d_pos=0.0733, pos_min=-100.0, freq_min=-6.823)
```

The user defined parameter set may not correspond to a uniquely solvable set of equations. In such cases, `FFTArray` guides the user to a working solution via its error messages. If the given constraints allow many different solutions, a `NoUniqueSolutionError` is thrown, suggesting additional parameters which could complete the set of constraints leading to a unique solution.

<sup>2</sup>Whether an output is printed as well as the shown output are not necessarily identical to what one would see in the real CPython interpreter REPL. We sometimes added the output of the assigned value which is normally not printed, switched the `__repr__` with the `__str__` representation and shortened floats in order to aid understanding.

<sup>3</sup>The REPL outputs in this section omit the `dynamically_traced_coords=False` member of the `Dimension` class and round floats to more readable lengths for pedagogical reasons.

Math	Name in Code	Description
$1 = N \Delta f \Delta x, \quad N \in \mathbb{N}_+$	n	Number of grid points
$\Delta x$	d_pos	Spacing between two grid points in position space.
$\Delta f$	d_freq	Spacing between two grid points in frequency space. If the unit of position space is $[x]$ , the unit in frequency space is its inverse $[f] = [x]^{-1}$ . This is a rotational frequency in cycles as opposed to an angular frequency.
$x_{\min}$	pos_min	The smallest position grid point.
$x_{\max} = x_{\min} + (N - 1) \Delta x$	pos_max	The largest position grid point.
$x_{\text{middle}} = \begin{cases} 0.5(x_{\min} + x_{\max} + \Delta x), & N \text{ even} \\ 0.5(x_{\min} + x_{\max}), & N \text{ odd} \end{cases}$	pos_middle	The middle of the position grid.
$x_{\text{extent}} = x_{\max} - x_{\min}$	pos_extent	The length of the position grid. Note that this is one $\Delta x$ smaller than the period $x_{\text{period}}$ .
$f_{\min}$	freq_min	The smallest frequency grid point.
$f_{\max} = f_{\min} + (N - 1) \Delta f$	freq_max	The largest frequency grid point.
$f_{\text{middle}} = \begin{cases} 0.5(f_{\min} + f_{\max} + \Delta f), & N \text{ even} \\ 0.5(f_{\min} + f_{\max}), & N \text{ odd} \end{cases}$	freq_middle	The middle of the frequency grid.
$f_{\text{extent}} = f_{\max} - f_{\min}$	freq_extent	The length of the frequency grid. Note that this is one $\Delta f$ smaller than the period $f_{\text{period}}$ .

Table 1: All parameters of the constraint system between position and frequency space. Math is the naming in section 2 while Code lists the naming adopted in the actual source code. Those names were chosen such that they are independent of the name of the used dimension to properly support multi-dimensional use-cases.

If, on the other hand, the given constraints have no solution at all, a `NoSolutionFoundError` suggests parameters to be removed. The solver also supports cases where an exact solution would require a non-integer number of grid points. In this case the error message suggests which parameters could be marked as `loose_params` to be automatically adapted. These parameters are then adapted such that  $N$  is even or a power of two. Rounding up means that the extent of a space is always increased and the spacing of samples decreased. Below we give an example, where  $\Delta x$  has been decreased such that it fits the constraints of  $\Delta x \leq 0.1$  and  $N$  being a power of two:

```

1  >>> fa.dim_from_constraints("x", d_pos=0.1, d_freq=0.05, pos_min=-9.,
2    ↵  freq_min=-6.4, n="power_of_two", loose_params=[d_pos])
2  Dimension(name='x', n=256, d_pos=0.078125, pos_min=-9.0, freq_min=-6.4)

```

Finally, the grid coordinates can be output as NumPy arrays with `dim.values(space)` or directly packed into a new `Array` via `fa.coords_from_dim(dim, space)` (cf. section 3.2.1).

### 3.2 The Array class: Managing Values in Position and Frequency Space

The `Array` class streamlines the handling of the gd(I)FT by automatically managing dimension-wise scale and phase factors in both, position and frequency space. This eliminates the need for the user to manually track coordinate grid compatibility and apply factors when combining multidimensional arrays with each other.

In contrast to a naive implementation like functions acting directly on NumPy arrays, which would redundantly apply scale and phase factors even when unnecessary, the `Array` class avoids such inefficiencies by tracking the current space of each `Dimension` and enabling transformations between spaces (see section 3.2.2). It automatically applies the correct factors only when required and elides them during arithmetic operations where possible (see sections 3.2.3 and 3.3). It does so by encapsulating the samples of a multidimensional function together with each `Dimension`. Correct dimension broadcasting and tracking of `Dimension` objects is enabled by associating each dimension with a unique name, similar to Unidata's self-describing Common Data Model, netCDF and xarray [31–33].

As outlined in section 3.4, the operations of the `Array` class are built upon the Python `Array` API [29] to enable portability with different array libraries and support computations on GPUs.

#### 3.2.1 Initialization

The `Array` class handles the gd(I)FT by storing the function values, the `Dimension` object and the current space for each dimension. It can be initialized in various ways depending on the use case; here we highlight the two most important ones. For a complete list of initialization functions we refer to the API reference in the documentation [34]. The most common way to initialize an `Array` is to directly fill it with the coordinate values of a `Dimension`:

```

1  >>> dim_x: fa.Dimension = fa.dim("x", pos_min=-0.1, freq_min=0., d_pos=0.2, n=4)
2  Dimension(name='x', n=4, d_pos=0.2, pos_min=-0.1, freq_min=0.0)
3  # convert the Dimension into an Array with values given by the coordinate grid:
4  ↵  g(x) = x
5  >>> arr_x: fa.Array = fa.coords_from_dim(dim_x, "pos")
6  <fftnarray.Array (x: 2^2)> Size: 32 bytes
7  |dimension| space | d | min | middle | max | extent |
8  +-----+-----+-----+-----+-----+-----+-----+
9  | x | pos | 0.20 | -0.10 | 0.30 | 0.50 | 0.60 |
10 |Values<array_api_compat.numpy>:
11 [-0.1 0.1 0.3 0.5]

```

After its initialization, the `Array` can be used in any arithmetic expression like for example `x**2`. Alternatively, one can wrap a preexisting bare array via `fa.array` with `Dimension` objects and define its current space:

```

1  >>> import numpy as np
2  >>> dim_x = fa.dim("x", pos_min=-0.1, freq_min=0., d_pos=0.2, n=4)
3  Dimension(name='x', n=4, d_pos=0.2, pos_min=-0.1, freq_min=0.0)
4  >>> np_values = np.array([5., 6., 7., 8.]) # correspond to the coordinate defined by
5  ← dims
6  >>> arr_pos = fa.array(np_values, [dim_x], "pos") # 1d Array in position space
7  <fftarray.Array (x: 2^2)> Size: 32 bytes
8  |dimension | space | d | min | middle | max | extent |
9  +-----+-----+-----+-----+-----+-----+-----+
10 | x | pos | 0.20 | -0.10 | 0.30 | 0.50 | 0.60 |
11 Values<array_api_compat.numpy>:
[5. 6. 7. 8.]

```

Instances of `Array` can hold all data types of the Python Array API Standard 2024.12 [29].

### 3.2.2 Fourier Transforms

A key design goal of `FFTArray` is to make the user deliberately select the required position or frequency space representation rather than explicitly executing transforms. The space for each dimension can be set individually and will trigger a `gd(I)FT` on the internal values. Thereby, the code automatically documents clearly which representation is used for each operation while the actual execution of the `gd(I)FT` becomes implicit and can be skipped if it is unnecessary.

```

1 arr_freq = arr_pos.into_space("freq") # change space: "pos" -> "freq"
2 arr_pos = arr_freq.into_space("pos") # change space: "freq" -> "pos"
3 arr_pos = arr_pos.into_space("pos") # No operation done because unnecessary.

```

Changing the space is only possible on a floating point `Array`. When performing space-changing operations, a real valued `Array` is automatically upcast to a complex floating point format of the same precision. It is also possible to set different spaces per dimension. This can be useful when mixing dimensions like time and space within the same array, which are usually not transformed simultaneously.

### 3.2.3 Arithmetic Operations and Broadcasting

`FFTArray` enables writing down most computations very similarly to their analytic counterparts. The `fftarray` namespace contains all element-wise functions of the Python Array API standard [29] like `sin`, `multiply`, etc. These implementations of arithmetic operations are also used to support all common element-wise unary and binary Python operators between `Array` instances as well as with scalars. Statistical functions like `sum` or `max` work with dimension names instead of axes indices and `integrate` additionally uses the spacings  $\Delta x$  and  $\Delta f$  stored in `Dimension` as integration elements.

When combining multiple arrays in an arithmetic operation their values and metadata are automatically aligned and broadcast by their `Dimension` name. The coordinate grids and space of equally named dimensions must exactly match between all operands. Because the results of an arithmetic operation differ when done in a different space there is no automatic conversion between position and frequency space.

The following example showcases a combination of the aforementioned features to define a two-dimensional Gaussian function:

```

1  >>> dim_x = fa.dim_from_constraints("x", pos_min=-1., pos_max=0., n=2,
2      ↵ freq_middle=0.)
3  >>> dim_y = fa.dim_from_constraints("y", pos_min=-2., pos_max=1., n=4,
4      ↵ freq_middle=0.)
5  >>> arr_x = fa.coords_from_dim(dim_x, "pos")
6  >>> arr_y = fa.coords_from_dim(dim_y, "pos")
7  >>> arr_gauss_2d = fa.exp(-(arr_x**2 + arr_y**2)/0.2) # same width along x and y,
8      ↵ centered around (x,y)=(0,0)
9  <fftwarray.Array (x: 2^1, y: 2^2)> Size: 64 bytes
10 |dimension | space | d | min | middle | max | extent |
11 +-----+-----+-----+-----+-----+-----+-----+
12 | x | pos | 1.00 | -1.00 | 0.00e+00 | 0.00e+00 | 1.00 |
13 | y | pos | 1.00 | -2.00 | 0.00e+00 | 1.00 | 3.00 |
14 Values<array_api_compat.numpy>:
15 [[1.389e-11 4.540e-05 6.738e-03 4.540e-05]
16 [2.061e-09 6.738e-03 1.000e+00 6.738e-03]]

```

Note that for all operations, the Dimension objects are properly stored in the resulting Array so that the Gaussian array can be easily transformed from position into frequency space with `arr_gauss_2d.into_space("freq")`.

### 3.2.4 Indexing

Indexing is supported via index or coordinate in any of the dimensions, similar to xarray.

```

1  # Select the point in the middle of both x and y direction.
2  >>> arr_gauss_2d.sel({"x": dim_x.pos_middle, "y": dim_y.pos_middle},
3      ↵ method="nearest")
4  <fftwarray.Array (x: 2^0, y: 2^0)> Size: 8 bytes
5  |dimension | space | d | min | middle | max | extent |
6  +-----+-----+-----+-----+-----+-----+-----+
7  | x | pos | 1.00 | 0.00e+00 | 0.00e+00 | 0.00e+00 | 0.00e+00 |
8  | y | pos | 1.00 | 0.00e+00 | 0.00e+00 | 0.00e+00 | 0.00e+00 |
9  Values<array_api_compat.numpy>:
10 [[1.]]

```

When slicing, the Dimensions are sliced as well and automatically used in the resulting Array. Slicing off a part of position space increases the value of `d_freq`, and conversely, slicing off a part of frequency space increases the value of `d_pos` due to their reciprocal relationship in eq. (11).

```

1  # Select the first 3 points in y dimension.
2  # The Dimension object is automatically adjusted to correctly cover the selected
3  ↵ points.
4  >>> arr_gauss_2d.isel({"y": slice(0,3)})
5  <fftwarray.Array (x: 2^1, y: 3)> Size: 48 bytes
6  |dimension | space | d | min | middle | max | extent |
7  +-----+-----+-----+-----+-----+-----+-----+
8  | x | pos | 1.00 | -1.00 | 0.00e+00 | 0.00e+00 | 1.00 |
9  | y | pos | 1.00 | -2.00 | -1.00 | 0.00e+00 | 2.00 |
10 Values<array_api_compat.numpy>:
11 [[1.389e-11 4.540e-05 6.738e-03]
12 [2.061e-09 6.738e-03 1.000e+00]]

```

Indexing with sub steps is not supported because the domain of the other space could be adjusted in multiple ways. Increasing the step size in one space reduces the extent of the other space. This extent reduction could be done on either end of the space or on both ends in different ways. Since there is no sensible default for this reduction, sub steps are not supported.

### 3.3 Lazy Phase Factor Application

One of the major design goals for FFTArray is to achieve high computational performance by avoiding unnecessary computations, particularly the application of scale and phase factors during gd(I)FTs. FFTArray can skip applying these factors if they would cancel out during back-and-forth transformations. The user-accessible values are always given in the representation with all phase and scale factors applied. Skipping certain factors in-between operations avoids floating-point inaccuracies which could otherwise accumulate if the factors were actually applied and reversed on each transform. Users retain control over this behavior as part of the programming model: if desired, they can explicitly influence or disable it. This explicit control ensures predictable outcomes, as opposed to relying on automatic optimizations, which may vary unpredictably across program versions or configurations.

In order to automate the scale and phase factor application while still ensuring user control, we introduce the concept of “lazy application”. After performing an (i)FFT using `into_space`, the scale and phase factors are not directly applied but instead, the resulting Array tracks that they are missing via the flag `factors_applied=False`. This flag is separate for each dimension. All operations on Array objects in FFTArray take `factors_applied` into account to ensure the correct result and avoid applying these factors if possible.

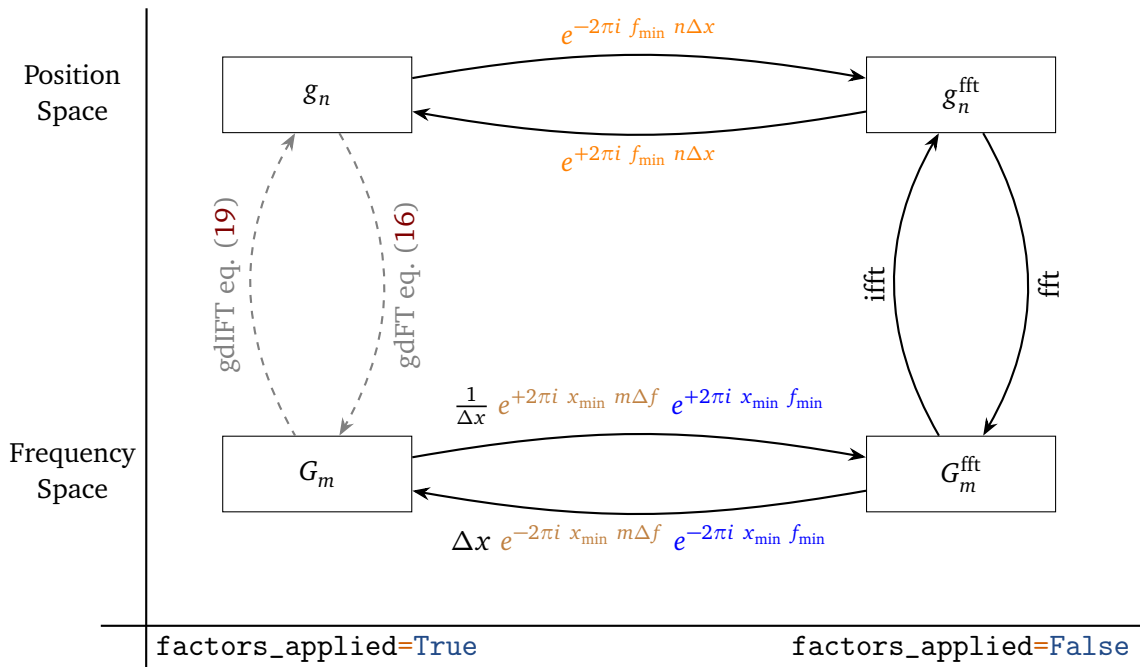


Figure 2: The four different internal states for the values of an FFTArray. By default (`eager=False`) each operation on the FFTArray minimizes the number of state transitions.

The flag `factors_applied` implements a new set of Arrays internal values on top of the current space flag, namely,  $g_n^{\text{fft}}$  and  $G_m^{\text{fft}}$ . The new states are required directly before computing the (I)FFT and are derived from eqs. (16) and (19) with the colored phase factors being the same. They are called  $g_n^{\text{fft}}$  and  $G_m^{\text{fft}}$ :

$$g_n^{\text{fft}} := g_n e^{-2\pi i f_{\min} n \Delta x}, \quad (28)$$

$$G_m^{\text{fft}} := G_m e^{+2\pi i x_{\min} m \Delta f} e^{+2\pi i x_{\min} f_{\min}} / \Delta x. \quad (29)$$

With these definitions, the gd(I)FT from  $g_n$  to  $G_m$  or vice versa can be split into three separate steps as depicted in fig. 2. For the gdFT, the first step is multiplying the position space values

$g_n$  with  $e^{-2\pi i f_{\min} n \Delta x}$ , which results in  $g_n^{\text{fft}}$ . The second step is performing the FFT on  $g_n^{\text{fft}}$  to compute  $G_m^{\text{fft}}$ . In the third step, we multiply  $G_m^{\text{fft}}$  with  $e^{+2\pi i x_{\min} m \Delta f} e^{+2\pi i x_{\min} f_{\min}} / \Delta x$  to get the actual frequency space values  $G_m$ . The advantage of splitting this process into three individual steps is that the final transitions  $g_n^{\text{fft}}$  to  $g_n$  ( $G_m^{\text{fft}}$  to  $G_m$ ) to the states with all phase factors applied can be skipped or simplified for many operations as shown in sections 3.3.1 to 3.3.4.

By default, the lazy evaluation minimizes state transitions in `factors_applied` in fig. 2 for all `Array` operations. The user can deactivate this behavior by setting the attribute `eager` to `True` for each dimension. In this case, the phase and scale factors are applied directly after each space change. Combining two `Array` instances raises an error if their `eager` attributes do not match.

All operations behave, up to numerical accuracy, as if they had been executed with the phase and scale factors applied. An `Array` object (`arr`) only allows public access to  $g_n$  (`arr.values("pos")`) and  $G_m$  (`arr.values("freq")`). In cases in which multiple calculations require the factors to be applied to the same `Array` it can improve performance to explicitly change the value of `factors_applied` with `arr = arr.into_factors_applied(True)`.

In order to take advantage of the lazy phase factor application, the functions `abs`, `add`, `subtract`, `multiply` and `divide` use optimized code paths. These optimized implementations apply to both the free-standing functions in the `fftarray` name space as well as their unary and binary counterparts on the `Array` class. Apart from `abs`, the above functions require two `Array` objects  $g_n$  and  $h_n$  as arguments and thus need separate rules for each combination of `factors_applied`. This chapter only focuses on a single dimension since phase and scale factor application is independent for each dimension. Additionally it only focuses on position space, since except for `abs` the same rules apply to frequency space just with the other phase and scale factors from eqs. (28) and (29).

The values stored internally in an `Array` are given by

$$g_n^{\text{int}}(s) := \begin{cases} g_n & \text{if } \text{factors\_applied} = \text{True} \\ g_n^{\text{fft}} & \text{if } \text{factors\_applied} = \text{False} \end{cases} = g_n [e^{-2\pi i f_{\min} n \Delta x}]^s, \quad (30)$$

using 28. In order to be able to write `factors_applied` in analytical expressions, we encode it into a variable  $s$ :

$$s := \begin{cases} 0 & \text{if } \text{factors\_applied} = \text{True} \\ 1 & \text{if } \text{factors\_applied} = \text{False} \end{cases}. \quad (31)$$

The correct full representation is obtained via moving the exponential to the other side:

$$g_n = g_n^{\text{int}}(s) [e^{+2\pi i f_{\min} n \Delta x}]^s. \quad (32)$$

### 3.3.1 Addition and subtraction

Addition has two input arrays with user-facing values  $g_n$  and  $h_n$  which should be added to get the result  $f_n := g_n + h_n$ . The derivation of the optimized rules for addition starts in terms of the two internal `Array` values  $g_n^{\text{int}}(s_1)$  and  $h_n^{\text{int}}(s_2)$  with their respective `factors_applied` states  $s_1$  and  $s_2$ . It is not always possible to completely avoid the application of scale and phase factors and still get a result of the form  $f_n^{\text{int}}(s^{\text{res}})$  with  $s^{\text{res}} \in \{0, 1\}$ . Therefore we introduce possible adjustments to each input as  $s_1^{\text{op}}, s_2^{\text{op}} \in \{-1, 0, 1\}$ . These adjustments can be used to switch the representation of the values in the `array` object between  $g_n$  and  $g_n^{\text{fft}}$  before the

eager	$s_1$	$s_2$	$s_1^{\text{op}}$	$s_2^{\text{op}}$	$s^{\text{res}} = s_1 + s_1^{\text{op}} = s_2 + s_2^{\text{op}}$
False	1	1	0	0	1
False	1	0	0	1	1
False	0	1	1	0	1
False	0	0	0	0	0
True	1	1	0	0	1
True	1	0	-1	0	0
True	0	1	0	-1	0
True	0	0	0	0	0

Table 2: Look-up-table for add and subtract. It encodes which inputs need phase and scale factors applied for each dimension. If possible the factors are factored out. `eager` acts as a tie breaker when any of the two inputs could be adjusted in order to get a correct result.

operation. For addition this results in:

$$g_n^{\text{int}}(s_1) \left[ e^{-2\pi i f_{\min} n \Delta x} \right]^{s_1^{\text{op}}} + h_n^{\text{int}}(s_2) \left[ e^{-2\pi i f_{\min} n \Delta x} \right]^{s_2^{\text{op}}} = g_n \left[ e^{-2\pi i f_{\min} n \Delta x} \right]^{s_1 + s_1^{\text{op}}} + h_n \left[ e^{-2\pi i f_{\min} n \Delta x} \right]^{s_2 + s_2^{\text{op}}} \quad (33)$$

$$= f_n \left[ e^{-2\pi i f_{\min} n \Delta x} \right]^{s^{\text{res}}}, \quad f_n := g_n + h_n \quad (34)$$

$$\Rightarrow s^{\text{res}} = s_1 + s_1^{\text{op}} = s_2 + s_2^{\text{op}}. \quad (35)$$

Now we need to solve eq. (35) while keeping  $s_1^{\text{op}} = 0$  and  $s_2^{\text{op}} = 0$  as much as possible in order to avoid having to apply phase and scale factors to the input operands. In the case of  $s_1 = s_2$  this is directly possible with  $s_1^{\text{op}} = s_2^{\text{op}} = 0$  leading to  $s^{\text{res}} = s_1 = s_2$ . If  $s_1 \neq s_2$ , one of the two input Arrays needs to be adjusted, so either  $s_1^{\text{op}} \neq 0$  or  $s_2^{\text{op}} \neq 0$ . Since the choice whether to adjust  $s_1$  or  $s_2$  has no performance implications, the `eager` attribute acts as a tie breaker. If `eager=False`,  $s_1^{\text{op}}$  and  $s_2^{\text{op}}$  are chosen such that  $s^{\text{res}} = 1$  which corresponds to `factors_applied=False`. If `eager=True`<sup>4</sup>, the  $s_1^{\text{op}}$  and  $s_2^{\text{op}}$  are chosen such that  $s^{\text{res}} = 0$  and therefore the resulting array will have `factors_applied=True`. The logic outlined above is encoded in table 2. These lookup tables are also used to implement that logic for each operation in the actual library. In each operation they are consulted for each dimension separately. The above derivation can be done identically for subtraction.

### 3.3.2 Multiplication

In the case of `multiply` the commutativity of complex multiplication can be exploited. The multiplication of two arrays  $g_n$  and  $h_n$  can be written as

<sup>4</sup>In this case `factors_applied=False` is pretty uncommon because it requires that the user manually changed either the `factors_applied` or `eager` attribute. But for example manually setting `factors_applied=False` on an `Array` with `eager=True` is a valid operation.

eager	$s_1$	$s_2$	$s_1^{\text{op}}$	$s_2^{\text{op}}$	$s^{\text{res}} = s_1 + s_1^{\text{op}} + s_2 + s_2^{\text{op}}$
False/True	1	1	0	-1	1
False/True	1	0	0	0	1
False/True	0	1	0	0	1
False/True	0	0	0	0	0

Table 3: Look-up-table for `multiply`. It encodes which inputs need phase and scale factors applied for each dimension. Since the multiplication of the inputs commutes with the factors, they can be propagated through without applying them except in the case of two phase factors which require the application of one of them.

$$g_n^{\text{int}}(s_1) \left[ e^{-2\pi i f_{\min} n \Delta x} \right]^{s_1^{\text{op}}} \times h_n^{\text{int}}(s_2) \left[ e^{-2\pi i f_{\min} n \Delta x} \right]^{s_2^{\text{op}}} \quad (36)$$

$$= g_n \left[ e^{-2\pi i f_{\min} n \Delta x} \right]^{s_1 + s_1^{\text{op}}} \times h_n \left[ e^{-2\pi i f_{\min} n \Delta x} \right]^{s_2 + s_2^{\text{op}}} \quad (37)$$

$$= (g_n \times h_n) \left[ e^{-2\pi i f_{\min} n \Delta x} \right]^{s_1 + s_1^{\text{op}} + s_2 + s_2^{\text{op}}} \quad (38)$$

$$\stackrel{!}{=} f_n \left[ e^{-2\pi i f_{\min} n \Delta x} \right]^{s^{\text{res}}}, \quad f_n := g_n \times h_n \quad (38)$$

$$\Rightarrow s^{\text{res}} \stackrel{!}{=} s_1 + s_1^{\text{op}} + s_2 + s_2^{\text{op}}. \quad (39)$$

Table 3 solves the resulting eq. (39) such that it minimizes the number of entries where  $s_j^{\text{op}} \neq 0$  and therefore also minimizes the amount of additional arithmetic. Only the case of  $s_1 = s_2 = 1$  requires the application of additional phase factors, which we have arbitrarily chosen to apply to the second Array.

### 3.3.3 Division

Division is similar to multiplication but with the difference that the signs of  $s_2$  and  $s_2^{\text{op}}$  in the equality condition for  $s^{\text{res}}$  are flipped:

$$\frac{g_n^{\text{int}}(s_1) \left[ e^{-2\pi i f_{\min} n \Delta x} \right]^{s_1^{\text{op}}}}{h_n^{\text{int}}(s_2) \left[ e^{-2\pi i f_{\min} n \Delta x} \right]^{s_2^{\text{op}}}} = \frac{g_n \left[ e^{-2\pi i f_{\min} n \Delta x} \right]^{s_1 + s_1^{\text{op}}}}{h_n \left[ e^{-2\pi i f_{\min} n \Delta x} \right]^{s_2 + s_2^{\text{op}}}} \quad (40)$$

$$= \frac{g_n}{h_n} \left[ e^{-2\pi i f_{\min} n \Delta x} \right]^{s_1 + s_1^{\text{op}} - s_2 - s_2^{\text{op}}} \quad (41)$$

$$\stackrel{!}{=} f_n \left[ e^{-2\pi i f_{\min} n \Delta x} \right]^{s^{\text{res}}}, \quad f_n := \frac{g_n}{h_n} \quad (42)$$

$$\Rightarrow s^{\text{res}} := s_1 + s_1^{\text{op}} - s_2 - s_2^{\text{op}}. \quad (43)$$

Solving eq. (43) in table 4 also requires an extra phase factor in only in one case. Again the operand can be chosen arbitrarily, though one needs to take care to use the correct sign.

### 3.3.4 Absolute values

`abs(x)` removes the phase of a complex number. Therefore, any not yet-applied phase-factors can simply be dropped and the result will always be with `factors_applied=True`. If the values are in frequency space and `factors_applied=False`, the scale factor  $[\Delta f N]^s$  needs to be applied before or after computing the absolute value of the internal values.

The frequency space scale factors  $[\Delta f N]^s$  are computed after the `abs` operation, because it is more efficient to apply them to a real-valued array instead of a complex-valued array.

eager	$s_1$	$s_2$	$s_1^{\text{op}}$	$s_2^{\text{op}}$	$s^{\text{res}} = s_1 + s_1^{\text{op}} - s_2 - s_2^{\text{op}}$
False/True	1	1	0	0	0
False/True	1	0	0	0	1
False/True	0	1	0	-1	0
False/True	0	0	0	0	0

Table 4: Look-up-table for divide. It encodes which inputs need phase and scale factors applied for each dimension. Compared to multiply the signs of the second operand are flipped but still only one case needs an actual correction to implement the operation correctly.

### 3.3.5 Showcase

The logic described in this section can be used to elide the application of phase and scale factors in a wide class of algorithms, which we demonstrate in section 4. Below we showcase a compact implementation of these optimizations.

```

1 import fftarray as fa
2
3 # Compute the dimension properties.
4 dim_x = fa.dim_from_constraints("x", pos_min=-1., pos_max=1., n=1024,
5                                freq_middle=0.)
6
7 # Initialize the coordinate grids in position and frequency space.
8 # Those are real-valued and therefore have to have factors_applied=True.
9 # They default to eager=False.
10 arr_x = fa.coords_from_dim(dim_x, "pos") # g_n
11 arr_f = fa.coords_from_dim(dim_x, "freq") # G_m
12
13 # The result of the square with factors_applied=True is again factors_applied=True
14 arr_pos1 = arr_x**2 # g_n
15 # Changing the space leaves the array with factors_applied=False. The factors have
16 # not been applied yet.
17 arr_freq1 = arr_pos1.into_space("freq") # G_m^fft
18
19 arr_freq2 = arr_freq1 * arr_f # G_m^fft, multiplication of factors_applied=False and
20 # factors_applied=True leads to factors_applied=False, no factors are actually
21 # applied during this operation.
22
23 # Because arr_freq2 is in the fft representation (G^fft_m) the ifft can be applied
24 # directly.
25 # Therefore this is only a call to ifft, no factors in frequency or position space
26 # necessary before the transformation.
27 arr_pos2 = arr_freq2.into_space("pos") # g_n^fft
28 # eager=False acts as a tie breaker, so the result has factors_applied=False.
29 arr_freq3 = arr_freq2 + 5 # G_m^fft, if eager=True it would be G_m
30
31 arr_freq3 = fa.exp(arr_freq2) # G_m, factors applied before exponential function
32 np_arr_freq2 = arr_freq2.values("freq") # values of G_m in a plain NumPy array
33
34 arr_freq4 = fa.abs(arr_freq2) # G_m, only scaling factors were applied since
35 # |G_m| = Δx|G_m^fft|

```

## 3.4 Python Array API

FFTArray is built on top of the Python Array API to leverage the speed-ups offered by modern hardware accelerators like GPUs. The specific needs of hardware accelerators for deep learning

and scientific compute led in the last years to the creation of multiple new python libraries for array computing. Each of these libraries has different trade-offs. NumPy is almost universally available in the Python ecosystem and has low start-up and per operation overhead. JAX and PyTorch both enable significant speed-ups on GPUs but have different designs and methods to translate a Python program to run on a GPU. A library like FFTArray is in principle agnostic to these details and could be built on top of any of these libraries. But the different trade-offs and histories of these libraries cause them to have different application programming interfaces (APIs). To enable a library like FFTArray to take advantage of all of these libraries from a single source, the Python Array API standard was created. It is developed by the Consortium for Python Data API Standards [29] and defines a common minimal set of functionality. Adoption of this standard is facilitated by the `array-api-compat` library [35]. It provides a wrapper over libraries like NumPy, PyTorch and JAX to fix any standard-violating behavior of the individual array libraries.

All array operations in FFTArray, from basic arithmetic to (i)FFTs, are forwarded to the underlying library via `array-api-compat`. Every Array API compliant library provides a namespace which we will call `xp`. This namespace exposes at least a standardised set of functionality like `xp.sin` or `xp.fft.fftn`. Every arithmetic operation on an `Array` from direct additions to functions like `fa.sin` are automatically dispatched to the functions of the Array API namespace `xp` of the array. As an example `fa.sin(arr).values("pos")` is equivalent to `xp.sin(arr.values("pos"))`. This also means that `array-api-compat` and the wrapped array library define any not standardized behavior of FFTArray. A notable example for not standardized behavior which is commonly used are the generally more relaxed type promotion rules. For example `np.asarray(True)+2` results in 3 with NumPy although this upcasting behavior (`bool` to `int`) is not guaranteed by the standard. When using NumPy as the backend for FFTArray this upcast is performed while with other backends it might not.

The array library can be different for each individual `Array`. An `Array` can be initialized with values from any Array API compatible library, e.g., `np.ndarray`. The Array API namespace is then automatically deduced. The other array creation functions can optionally be given an Array API namespace. If it is not possible to determine the used array library from the input like in the case of a list, FFTArray uses a user-configurable default namespace which itself defaults to NumPy. The Array API namespace of any `Array` can also always be inspected via `arr.xp` and changed via `new_arr = arr.into_xp(xp)`. This conversion behavior currently always goes through a NumPy array and only supports explicitly implemented libraries because it is not covered by the standard at the moment.

If the user attempts to mix multiple different namespaces, an error is thrown because it is unclear in which namespace the operation should be executed. Therefore, the user needs to ensure that all arrays which are combined in an operation use the same underlying array library. In the example below, we show how to set it to the `jax.numpy` namespace. In this case, any operations on the arrays `arr_g_x_jax` or `arr_lin_jax` are executed by JAX.

```

1  >>> import jax.numpy as jnp
2  >>> import fftarray as fa
3  >>> dim_x = fa.dim_from_constraints("x", pos_min=-1., pos_max=1., n=4,
4  >   freq_middle=0.)
5
6  >>> arr_g_x_jax = fa.coords_from_dim(dim_x, "pos", xp=jnp) # set namespace
7  >   explicitly to jax.numpy
8  <fftarray.Array (x: 2^2)> Size: 16 bytes
9  |dimension | space | d | min | middle | max | extent |
10 |-----+-----+-----+-----+-----+-----+-----+
11 | x | pos | 0.67 | -1.00 | 0.33 | 1.00 | 2.00 |
12 Values<jax.numpy>:
13 [-1. -0.3333333 0.33333337 1.]

```

```

12
13 >>> arr_lin_jax = fa.array(jnp.linspace(0., 1.5, 4), dim_x, "pos")
14 <fftarray.Array (x: 2^2)> Size: 16 bytes
15 |dimension | space | d | min | middle | max | extent |
16 +-----+-----+-----+-----+-----+-----+-----+
17 | x | pos | 0.67 | -1.00 | 0.33 | 1.00 | 2.00 |
18 Values<jax.numpy>:
19 [0. 0.5 1. 1.5]

```

### 3.4.1 JAX Tracing

The tracing feature of JAX is often required to reach high computational performance when using JAX as the `xp`. Tracing extracts the computation graph of a Python function by executing it with placeholder values that retain only the shape and data type of arrays, not their actual values. This graph is then compiled for efficient execution, particularly on GPUs. It can also be modified to enable features like gradient computation. For tracing to work, JAX requires custom types (e.g. `Array` and `Dimension`) to mark which members are dynamic (replaced by placeholders) and which are static during computation.

`FFTArray` supports JAX tracing by providing the necessary implementations. Users must register `Array` and `Dimension` as JAX-compatible data structures by calling `fa.jax_register_pytree_nodes()` before use.

By default, all members of the `Dimension` class are marked as static during tracing. This inserts all member values directly into the generated computation graph, enabling efficient reuse of compiled code (e.g., in loops). However, this prevents dynamic updates to grids during execution, as changes would require re-tracing the function. To enable dynamic grids (e.g., for moving domains) the creation functions of `Dimension` have the parameter `dynamically_traced_coords`. Setting it to `True` makes  $x_{\min}$ ,  $f_{\min}$  and  $\Delta x$  as well as all derived parameters except for  $N$  (since JAX requires fixed shapes) dynamic at trace time. This allows to reuse the same function for different `Dimensions` but comes with a restriction in usability. Since most properties of `Dimension` are dynamic in this case, it cannot be checked at trace time whether one `Dimension` is equal to another. Therefore if two arrays each contain a `Dimension` with the same name but different tracers, they cannot be combined with each other as shown below:

```

1 import pytest
2 import fftarray as fa
3 import jax
4 fa.jax_register_pytree_nodes()
5 fa.set_default_xp(jax.numpy)
6
7 dim_x = fa.Dimension("x", 4, 0.5, 0., 0., dynamically_traced_coords=True)
8
9 @jax.jit
10 def my_fun(dim1: fa.Dimension) -> fa.Array:
11     arr1 = fa.coords_from_dim(dim1, "pos")
12     arr2 = fa.coords_from_dim(dim1, "pos")
13
14     # Works, because both arrays use the same dimension with the same tracers.
15     return arr1+arr2
16
17 my_fun(dim_x)
18
19 @jax.jit
20 def my_fun_not_dynamic(dim1: fa.Dimension, dim2: fa.Dimension) -> fa.Array:
21     arr1 = fa.coords_from_dim(dim1, "pos")
22     arr2 = fa.coords_from_dim(dim2, "pos")

```

```
24 # Addition requires all dimensions with the same name to be equal, this is
25 # explicitly checked before the operation.
26 # The check for equality fails with a `jax.errors.TracerBoolConversionError`
27 # because the coordinate grids' values of the `Dimension`'s are only known at
28 # runtime.
29 # If `dynamically_traced_coords` above were set to False, the exact values of
30 # `dim1` and `dim2` were available at trace time and therefore this addition
31 # would succeed.
32 return arr1+arr2
33
34
35
36
37
38
39
40
41
42
43
44
45
46
47
48
49
50
51
52
53
54
55
56
57
58
59
60
61
62
63
64
65
66
67
68
69
70
71
72
73
74
75
76
77
78
79
80
81
82
83
84
85
86
87
88
89
90
91
92
93
94
95
96
97
98
99
100
101
102
103
104
105
106
107
108
109
110
111
112
113
114
115
116
117
118
119
120
121
122
123
124
125
126
127
128
129
130
131
132
133
134
135
136
137
138
139
140
141
142
143
144
145
146
147
148
149
150
151
152
153
154
155
156
157
158
159
160
161
162
163
164
165
166
167
168
169
170
171
172
173
174
175
176
177
178
179
180
181
182
183
184
185
186
187
188
189
190
191
192
193
194
195
196
197
198
199
200
201
202
203
204
205
206
207
208
209
210
211
212
213
214
215
216
217
218
219
220
221
222
223
224
225
226
227
228
229
230
231
232
233
234
235
236
237
238
239
240
241
242
243
244
245
246
247
248
249
250
251
252
253
254
255
256
257
258
259
259
260
261
262
263
264
265
266
267
268
269
269
270
271
272
273
274
275
276
277
278
279
279
280
281
282
283
284
285
286
287
288
289
289
290
291
292
293
294
295
296
297
298
299
299
300
301
302
303
304
305
306
307
308
309
309
310
311
312
313
314
315
316
317
318
319
319
320
321
322
323
324
325
326
327
328
329
329
330
331
332
333
334
335
336
337
338
339
339
340
341
342
343
344
345
346
347
348
349
349
350
351
352
353
354
355
356
357
358
359
359
360
361
362
363
364
365
366
367
368
369
369
370
371
372
373
374
375
376
377
378
379
379
380
381
382
383
384
385
386
387
388
389
389
390
391
392
393
394
395
396
397
398
399
399
400
401
402
403
404
405
406
407
408
409
409
410
411
412
413
414
415
416
417
418
419
419
420
421
422
423
424
425
426
427
428
429
429
430
431
432
433
434
435
436
437
438
439
439
440
441
442
443
444
445
446
447
448
449
449
450
451
452
453
454
455
456
457
458
459
459
460
461
462
463
464
465
466
467
468
469
469
470
471
472
473
474
475
476
477
478
479
479
480
481
482
483
484
485
486
487
488
489
489
490
491
492
493
494
495
496
497
498
499
499
500
501
502
503
504
505
506
507
508
509
509
510
511
512
513
514
515
516
517
518
519
519
520
521
522
523
524
525
526
527
528
529
529
530
531
532
533
534
535
536
537
538
539
539
540
541
542
543
544
545
546
547
548
549
549
550
551
552
553
554
555
556
557
558
559
559
560
561
562
563
564
565
566
567
568
569
569
570
571
572
573
574
575
576
577
578
579
579
580
581
582
583
584
585
586
587
588
589
589
590
591
592
593
594
595
596
597
598
599
599
600
601
602
603
604
605
606
607
608
609
609
610
611
612
613
614
615
616
617
618
619
619
620
621
622
623
624
625
626
627
628
629
629
630
631
632
633
634
635
636
637
638
639
639
640
641
642
643
644
645
646
647
648
649
649
650
651
652
653
654
655
656
657
658
659
659
660
661
662
663
664
665
666
667
668
669
669
670
671
672
673
674
675
676
677
678
679
679
680
681
682
683
684
685
686
687
688
689
689
690
691
692
693
694
695
696
697
697
698
699
700
701
702
703
704
705
706
707
708
709
709
710
711
712
713
714
715
716
717
718
719
719
720
721
722
723
724
725
726
727
728
729
729
730
731
732
733
734
735
736
737
738
739
739
740
741
742
743
744
745
746
747
748
749
749
750
751
752
753
754
755
756
757
758
759
759
760
761
762
763
764
765
766
767
768
769
769
770
771
772
773
774
775
776
777
778
779
779
780
781
782
783
784
785
786
787
788
788
789
789
790
791
792
793
794
795
796
797
797
798
799
799
800
801
802
803
804
805
806
807
808
809
809
810
811
812
813
814
815
816
817
818
819
819
820
821
822
823
824
825
826
827
828
829
829
830
831
832
833
834
835
836
837
838
839
839
840
841
842
843
844
845
846
847
848
849
849
850
851
852
853
854
855
856
857
858
859
859
860
861
862
863
864
865
866
867
868
869
869
870
871
872
873
874
875
876
877
878
879
879
880
881
882
883
884
885
886
887
888
888
889
889
890
891
892
893
894
895
896
897
897
898
899
899
900
901
902
903
904
905
906
907
908
909
909
910
911
912
913
914
915
916
917
918
919
919
920
921
922
923
924
925
926
927
928
929
929
930
931
932
933
934
935
936
937
938
939
939
940
941
942
943
944
945
946
947
948
949
949
950
951
952
953
954
955
956
957
958
959
959
960
961
962
963
964
965
966
967
968
969
969
970
971
972
973
974
975
976
977
978
978
979
979
980
981
982
983
984
985
986
987
987
988
988
989
989
990
991
992
993
994
995
996
997
997
998
999
999
1000
1000
1001
1002
1003
1004
1005
1006
1007
1008
1009
1009
1010
1011
1012
1013
1014
1015
1016
1017
1018
1019
1019
1020
1021
1022
1023
1024
1025
1026
1027
1028
1029
1029
1030
1031
1032
1033
1034
1035
1036
1037
1038
1039
1039
1040
1041
1042
1043
1044
1045
1046
1047
1048
1048
1049
1050
1051
1052
1053
1054
1055
1056
1057
1058
1059
1059
1060
1061
1062
1063
1064
1065
1066
1067
1068
1069
1069
1070
1071
1072
1073
1074
1075
1076
1077
1078
1078
1079
1079
1080
1081
1082
1083
1084
1085
1086
1087
1087
1088
1088
1089
1089
1090
1091
1092
1093
1094
1095
1096
1096
1097
1097
1098
1098
1099
1099
1100
1101
1102
1103
1104
1105
1106
1107
1108
1109
1109
1110
1111
1112
1113
1114
1115
1116
1117
1118
1119
1119
1120
1121
1122
1123
1124
1125
1126
1127
1128
1128
1129
1129
1130
1131
1132
1133
1134
1135
1136
1137
1138
1138
1139
1139
1140
1141
1142
1143
1144
1145
1146
1147
1147
1148
1148
1149
1149
1150
1151
1152
1153
1154
1155
1156
1157
1158
1158
1159
1159
1160
1161
1162
1163
1164
1165
1166
1167
1167
1168
1168
1169
1169
1170
1171
1172
1173
1174
1175
1176
1176
1177
1177
1178
1178
1179
1179
1180
1181
1182
1183
1184
1185
1186
1186
1187
1187
1188
1188
1189
1189
1190
1191
1192
1193
1194
1195
1195
1196
1196
1197
1197
1198
1198
1199
1199
1200
1201
1202
1203
1204
1205
1206
1207
1208
1208
1209
1209
1210
1211
1212
1213
1214
1215
1216
1216
1217
1217
1218
1218
1219
1219
1220
1221
1222
1223
1224
1225
1226
1226
1227
1227
1228
1228
1229
1229
1230
1231
1232
1233
1234
1235
1236
1236
1237
1237
1238
1238
1239
1239
1240
1241
1242
1243
1244
1245
1246
1246
1247
1247
1248
1248
1249
1249
1250
1251
1252
1253
1254
1255
1256
1256
1257
1257
1258
1258
1259
1259
1260
1261
1262
1263
1264
1265
1266
1266
1267
1267
1268
1268
1269
1269
1270
1271
1272
1273
1274
1275
1276
1276
1277
1277
1278
1278
1279
1279
1280
1281
1282
1283
1284
1285
1286
1286
1287
1287
1288
1288
1289
1289
1290
1291
1292
1293
1294
1295
1295
1296
1296
1297
1297
1298
1298
1299
1299
1300
1301
1302
1303
1304
1305
1306
1307
1308
1308
1309
1309
1310
1311
1312
1313
1314
1315
1316
1316
1317
1317
1318
1318
1319
1319
1320
1321
1322
1323
1324
1325
1326
1326
1327
1327
1328
1328
1329
1329
1330
1331
1332
1333
1334
1335
1336
1336
1337
1337
1338
1338
1339
1339
1340
1341
1342
1343
1344
1345
1346
1346
1347
1347
1348
1348
1349
1349
1350
1351
1352
1353
1354
1355
1356
1356
1357
1357
1358
1358
1359
1359
1360
1361
1362
1363
1364
1365
1366
1366
1367
1367
1368
1368
1369
1369
1370
1371
1372
1373
1374
1375
1376
1376
1377
1377
1378
1378
1379
1379
1380
1381
1382
1383
1384
1385
1386
1386
1387
1387
1388
1388
1389
1389
1390
1391
1392
1393
1394
1395
1395
1396
1396
1397
1397
1398
1398
1399
1399
1400
1401
1402
1403
1404
1405
1406
1407
1408
1408
1409
1409
1410
1411
1412
1413
1414
1415
1416
1416
1417
1417
1418
1418
1419
1419
1420
1421
1422
1423
1424
1425
1426
1426
1427
1427
1428
1428
1429
1429
1430
1431
1432
1433
1434
1435
1436
1436
1437
1437
1438
1438
1439
1439
1440
1441
1442
1443
1444
1445
1446
1446
1447
1447
1448
1448
1449
1449
1450
1451
1452
1453
1454
1455
1456
1456
1457
1457
1458
1458
1459
1459
1460
1461
1462
1463
1464
1465
1466
1466
1467
1467
1468
1468
1469
1469
1470
1471
1472
1473
1474
1475
1476
1476
1477
1477
1478
1478
1479
1479
1480
1481
1482
1483
1484
1485
1486
1486
1487
1487
1488
1488
1489
1489
1490
1491
1492
1493
1494
1495
1495
1496
1496
1497
1497
1498
1498
1499
1499
1500
1501
1502
1503
1504
1505
1506
1507
1508
1508
1509
1509
1510
1511
1512
1513
1514
1515
1516
1516
1517
1517
1518
1518
1519
1519
1520
1521
1522
1523
1524
1525
1526
1526
1527
1527
1528
1528
1529
1529
1530
1531
1532
1533
1534
1535
1536
1536
1537
1537
1538
1538
1539
1539
1540
1541
1542
1543
1544
1545
1546
1546
1547
1547
1548
1548
1549
1549
1550
1551
1552
1553
1554
1555
1556
1556
1557
1557
1558
1558
1559
1559
1560
1561
1562
1563
1564
1565
1566
1566
1567
1567
1568
1568
1569
1569
1570
1571
1572
1573
1574
1575
1576
1576
1577
1577
1578
1578
1579
1579
1580
1581
1582
1583
1584
1585
1586
1586
1587
1587
1588
1588
1589
1589
1590
1591
1592
1593
1594
1595
1595
1596
1596
1597
1597
1598
1598
1599
1599
1600
1601
1602
1603
1604
1605
1606
1607
1608
1608
1609
1609
1610
1611
1612
1613
1614
1615
1616
1616
1617
1617
1618
1618
1619
1619
1620
1621
1622
1623
1624
1625
1626
1626
1627
1627
1628
1628
1629
1629
1630
1631
1632
1633
1634
1635
1636
1636
1637
1637
1638
1638
1639
1639
1640
1641
1642
1643
1644
1645
1646
1646
1647
1647
1648
1648
1649
1649
1650
1651
1652
1653
1654
1655
1656
1656
1657
1657
1658
1658
1659
1659
1660
1661
1662
1663
1664
1665
1666
1666
1667
1667
1668
1668
1669
1669
1670
1671
1672
1673
1674
1675
1676
1676
1677
1677
1678
1678
1679
1679
1680
1681
1682
1683
1684
1685
1686
1686
1687
1687
1688
1688
1689
1689
1690
1691
1692
1693
1694
1695
1695
1696
1696
1697
1697
1698
1698
1699
1699
1700
1701
1702
1703
1704
1705
1706
1707
1708
1708
1709
1709
1710
1711
1712
1713
1714
1715
1716
1716
1717
1717
1718
1718
1719
1719
1720
1721
1722
1723
1724
1725
1726
1726
1727
1727
1728
1728
1729
1729
1730
1731
1732
1733
1734
1735
1736
1736
1737
1737
1738
1738
1739
1739
1740
1741
1742
1743
1744
1745
1746
1746
1747
1747
1748
1748
1749
1749
1750
1751
1752
1753
1754
1755
1756
1756
1757
1757
1758
1758
1759
1759
1760
1761
1762
1763
1764
1765
1766
1766
1767
1767
1768
1768
1769
1769
1770
1771
1772
1773
1774
1775
1776
1776
1777
1777
1778
1778
1779
1779
1780
1781
1782
1783
1784
1785
1786
1786
1787
1787
1788
1788
1789
1789
1790
1791
1792
1793
1794
1795
1795
1796
1796
1797
1797
1798
1798
1799
1799
1800
1801
1802
1803
1804
1805
1806
1807
1808
1808
1809
1809
1810
1811
1812
1813
1814
1815
1816
1816
1817
1817
1818
1818
1819
1819
1820
1821
1822
1823
1824
1825
1826
1826
1827
1827
1828
1828
1829
1829
1830
1831
1832
1833
1834
1835
1836
1836
1837
1837
1838
1838
1839
1839
1840
1841
1842
1843
1844
1845
1846
1846
1847
1847
1848
1848
1849
1849
1850
1851
1852
1853
1854
1855
1856
1856
1857
1857
1858
1858
1859
1859
1860
1861
1862
1863
1864
1865
1866
1866
1867
1867
1868
1868
1869
1869
1870
1871
1872
1873
1874
1875
1876
1876
1877
1877
1878
1878
1879
1879
1880
1881
1882
1883
1884
1885
1886
1886
1887
1887
1888
1888
1889
1889
1890
1891
1892
1893
1894
1895
1895
1896
1896
1897
1897
1898
1898
1899
1899
1900
1901
1902
1903
1904
1905
1906
1907
1908
1908
1909
1909
1910
1911
1912
1913
1914
1915
1916
1916
1917
1917
1918
1918
1919
1919
1920
1921
1922
1923
1924
1925
1926
1926
1927
1927
1928
1928
1929
1929
1930
1931
1932
1933
1934
1935
1936
1936
1937
1937
1938
1938
1939
1939
1940
1941
1942
1943
1944
1945
1946
1946
1947
1947
1948
1948
1949
1949
1950
1951
1952
1953
1954
1955
1956
1956
1957
1957
1958
1958
1959
1959
1960
1961
1962
1963
1964
1965
1966
1966
1967
1967
1968
1968
1969
1969
1970
1971
1972
1973
1974
1975
1976
1976
1977
1977
1978
1978
1979
1979
1980
1981
1982
1983
1984
1985
1986
1986
1987
1987
1988
1988
1989
1989
1990
1991
1992
1993
1994
1995
1995
1996
1996
1997
1997
1998
1998
1999
1999
2000
2001
2002
2003
2004
2005
2006
2007
2008
2008
2009
2009
2010
2011
2012
2013
2014
2015
2016
2016
2017
2017
2018
2018
2019
2019
2020
2021
2022
2023
2024
2025
2026
2027
2028
2029
2030
2031
2032
2033
2034
2035
2036
2037
2038
2038
2039
2039
2040
2041
2042
2043
2044
2045
2046
2046
2047
2047
2048
2048
2049
2049
2050
2051
2052
2053
2054
2055
2056
2056
2057
2057
2058
2058
2059
2059
2060
2061
2062
2063
2064
2065
2066
2066
2067
2067
2068
2068
2069
2069
2070
2071
2072
2073
2074
2075
2076
2076
2077
2077
2078
2078
2079
2079
2080
2081
2082
2083
2084
2085
2086
2086
2087
2087
2088
2088
2089
2089
2090
2091
2092
2093
2094
2095
2095
2096
2096
2097
2097
2098
2098
2099
2099
2100
2101
2102
2103
2104
2105
2106
2107
2108
2108
2109
2109
2110
2111
2112
2113
2114
2115
2116
2116
2117
2117
2118
2118
2119
2119
2120
2121
2122
2123
2124
2125
2126
2126
2127
2127
2128
2128
2129
2129
2130
2131
2132
2133
2134
2135
2136
2136
2137
2137
2138
2138
2139
2139
2140
2141
2142
2143
2144
2145
2146
2146
2147
2147
2148
2148
2149
2149
2150
2151
2152
2153
2154
2155
2156
2156
2157
2157
2158
2158
2159
2159
2160
2161
2162
2163
2164
2165
2166
2166
2167
2167
2168
2168
2169
2169
2170
2171
2172
2173
2174
2175
2176
2176
2177
2177
2178
2178
2179
2179
2180
2181
2182
2183
2184
2185
2186
2186
2187
2187
2188
2188
2189
2189
2190
2191
2192
2193
2194
2
```

This can be solved by passing each `Dimension` instance exactly once into the jitted function. Note that when passing the same `Dimension` object as part of two different `FFTArray` objects, each `Dimension` instance gets its own distinct tracer. For example two `FFTArray` objects which contain a `Dimension` named "`x`" could not be combined inside a jitted function if they were passed in as parameters. Using `dynamically_traced_coords=True` requires very careful engineering of the code. Therefore, it defaults to `False` to cover the more common cases of static coordinate grids.

## 4 Examples

In this section, we demonstrate applications of FFTArray using various examples where gdFTs come into play. Section 4.1 demonstrates how to numerically compute a derivative. Section 4.2 describes how to use the split-step Fourier method to solve the Schrödinger equation. This method is then used in section 4.3 to simulate a matter-wave beam splitter using Bragg diffraction. Section 4.4 and Section 4.5 use a variation of Fourier split-step called imaginary time evolution to find the ground state of matter waves in a harmonic trap. Section 4.4 implements a single species wave function without self-interaction in a two-dimensional isotropic harmonic oscillator and evaluates the precision of the solution against the precise analytic solution. Section 4.5 extends that to two interacting Bose-Einstein condensates in a harmonic trap.

## 4.1 Derivative

The Fourier transform can be used to compute the  $n$ -th order derivative of a function  $g(x) : \mathbb{R} \rightarrow \mathbb{C}$  with:

$$\frac{\partial^n}{\partial x^n} g(x) = \widehat{\mathcal{F}} \{(2\pi i f)^n \mathcal{F} \{g(x)\}\}. \quad (44)$$

Note that directly discretizing this relation as shown in this chapter is only one way to numerically compute a derivative and roughly equivalent to a highest-order difference formula. If the signal showcases strong discontinuities including at the periodic boundaries of the sampled domain, other approaches like a lower order differencing formula can lead to better results. Such approaches can also be implemented with an FFT by a convolution with a different kernel [36, 37]. We showcase the implementation of eq. (44) with a modulated

Gaussian and both its analytic and numeric derivative:

$$g(x) = \cos(x) e^{\frac{-(x-1.25)^2}{25}}, \quad (45)$$

$$\frac{\partial}{\partial x} g(x) = \left( \frac{-2(x-1.25)}{25} \cos(x) - \sin(x) \right) e^{\frac{-(x-1.25)^2}{25}}. \quad (46)$$

This test function and the x grid in the example code are both not symmetric around zero in order to show a general case where the phase factors cannot be simplified. An important property of the test function is that it goes to zero on the edges of the sampled domain. If one extends the domain on both sides to get values on the boundaries even closer to zero, the precision of the derivative increases further in this case. The analytical function and its derivative are plotted alongside their numerical counterparts in fig. 3.

```

1 import numpy as np
2 import fftarray as fa
3
4 # Test function and its derivative
5 g = lambda x: fa.cos(x)*fa.exp(-(x-1.25)**2/25.)
6 g_d1 = lambda x: ((-(2*(x-1.25))/25.)*fa.cos(x) -
7     fa.sin(x))*fa.exp(-(x-1.25)**2/25.)
8
9 dim_x = fa.dim_from_constraints("x", # dimension name
10     pos_min=-40., pos_max=50., d_pos=.5, # position space grid
11     freq_middle=0., # frequency grid offset
12     loose_params=["d_pos"], # The resulting d_pos in dim_x will be made smaller
13     # than the input d_pos such that N is a power of two.
14 )
15 x = fa.coords_from_dim(dim_x, "pos") # position space coordinate grid
16 f = fa.coords_from_dim(dim_x, "freq") # frequency space coordinate grid
17 sampled_fn = g(x) # sample the function in position space
18
19 # Compute the derivative
20 order = 1 # Order of the derivative
21 derivative_kernel = (2*np.pi*1.j*f)**order
22 g_d1_numeric = (sampled_fn.into_space("freq")*derivative_kernel).into_space("pos")
23
24
25 # Compute the expected result directly from the analytic derivative.
26 d1_analytic = g_d1(x)
27
28 # Compare the numeric and analytical result.
29 # In this example with these domains they are equal to at least eleven decimal
30 # digits.
31 np.testing.assert_array_almost_equal(g_d1_numeric.values("pos"),
32     d1_analytic.values("pos"), decimal=11)

```

The `assert` in line 27 shows that this example is precise to up to 11 decimal digits. If the zero padding on the sides is chosen larger, the precision can also be higher. In this example the cancellation of the phase factors (reduced to `fftshift` and `ifftshift`) in section 2.3.4 happens automatically in line 20.

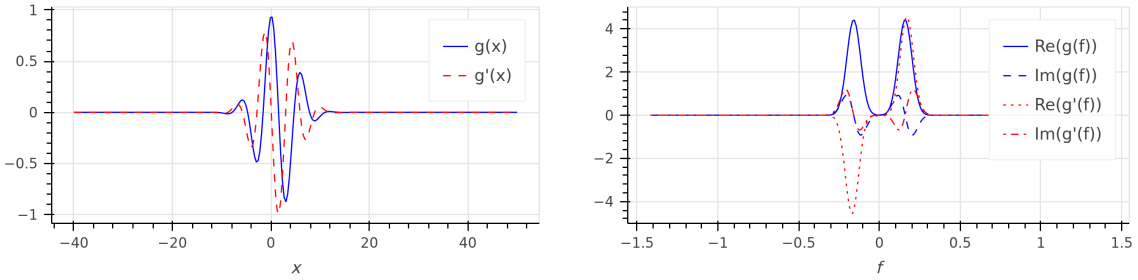


Figure 3: For illustration purposes a plot of the example function, eq. (45), and its first derivative, eq. (46), used to demonstrate differentiation using the gdFT. The left plot is in position space and the right plot in frequency space. Both are plotted in the exact domain and sample density used in the example code.

## 4.2 Solving the Schrödinger Equation

The Schrödinger equation is the central wave equation of quantum mechanics describing the time evolution of a single particle:

$$T_{\mathbf{r}} := \frac{-\hbar^2 \nabla_{\mathbf{r}}^2}{2m} \quad (47)$$

$$i\hbar \frac{\partial}{\partial t} \Psi(\mathbf{r}, t) = H(\mathbf{r}, t) \Psi(\mathbf{r}, t) \quad (48)$$

$$= (T_{\mathbf{r}} + V(\mathbf{r}, t)) \Psi(\mathbf{r}, t) \quad (49)$$

where  $T_{\mathbf{r}}$  is the kinetic energy operator and  $\Psi(\mathbf{r}, t) : (\mathbb{R}^n, \mathbb{R}) \rightarrow \mathbb{C}$  represents the particle's wave function in a (possibly) time-dependent potential  $V(\mathbf{r}, t) : (\mathbb{R}^n, \mathbb{R}) \rightarrow \mathbb{R}$ .  $m$  denotes the mass of the particle and  $\hbar$  is the reduced Planck constant.

The solution for the time propagation of the Schrödinger equation is the evolution operator  $U$ :

$$\Psi(\mathbf{r}, t + s) = U(t + s, t) \Psi(\mathbf{r}, t) \quad (50)$$

$$= \mathcal{T} \exp \left( -\frac{i}{\hbar} \int_t^{t+s} dt' s H(\mathbf{r}, t') \right) \Psi(\mathbf{r}, t) \quad (51)$$

$$\text{with } \mathcal{T}(A(t)B(t')) = \begin{cases} A(t)B(t'), & \text{if } t > t' \\ B(t')A(t), & \text{if } t < t' \end{cases} \quad (52)$$

Now we discretize the time evolution and only use very small time steps  $\Delta t$  under the assumption that the Hamiltonian does not change too much over that time span. For a fixed time  $t$  we get a time-independent  $H(\mathbf{r}, t)$  under which we evolve for some time step  $\Delta t$ :

$$U(t + \Delta t, t) \Psi(\mathbf{r}, t) \approx \exp \left( -\frac{i}{\hbar} H(\mathbf{r}, t) \Delta t \right) \Psi(\mathbf{r}, t). \quad (53)$$

To achieve a longer time evolution each of these time steps is repeated multiple times to approximate the target dynamics.

For many problems the analytical evaluation of this solution is impractical. To solve it numerically, the wave function and potential can be approximated by sampling the wave function in position space at a high resolution. Evaluating the derivative contained in  $H(\mathbf{r}, t)$  would then require a finite difference approximation. Exponentiating that finite difference approximation requires representing the resulting operator as a matrix with  $\mathcal{O}(N^2)$  elements for the size  $N$  of each dimension.

To avoid storing and multiplying matrices we can make use of eq. (44) and use a Fourier transform to turn the position derivative into a simple multiplication with  $\mathbf{f}$ :

$$\mathcal{F}(\nabla_{\mathbf{r}}^2 \Psi(\mathbf{r})) = (2\pi\mathbf{f})^2 \Psi(\mathbf{f}). \quad (54)$$

This process is called diagonalization and causes the matrix representation of the operator in our discrete basis to become diagonal and the exponential of a diagonal matrix is just the exponential of each of its diagonal element. However, the exponential also contains the potential operator. That operator is diagonal in position space and would become a non-diagonal derivative when transformed into frequency space. The evolution operator in eq. (53) can be split into an approximate product of three diagonal operators with a second order Trotter approximation, also called split-step or Strang-Splitting [1, 2]:

$$\begin{aligned} & \exp\left(-\frac{i}{\hbar}H(\mathbf{r}, t)\Delta t\right)\Psi(\mathbf{r}, t) \\ &= \exp\left(-\frac{i}{\hbar}V(\mathbf{r}, t)\frac{\Delta t}{2}\right)\exp\left(-\frac{i}{\hbar}T_{\mathbf{r}}\Delta t\right)\exp\left(-\frac{i}{\hbar}V(\mathbf{r}, t)\frac{\Delta t}{2}\right)\Psi(\mathbf{r}, t) + \mathcal{O}(\Delta t^3) \end{aligned} \quad (55)$$

or alternatively

$$\begin{aligned} & \exp\left(-\frac{i}{\hbar}H(\mathbf{r}, t)\Delta t\right)\Psi(\mathbf{r}, t) \\ &= \exp\left(-\frac{i}{\hbar}T_{\mathbf{r}}\frac{\Delta t}{2}\right)\exp\left(-\frac{i}{\hbar}V(\mathbf{r}, t)\Delta t\right)\exp\left(-\frac{i}{\hbar}T_{\mathbf{r}}\frac{\Delta t}{2}\right)\Psi(\mathbf{r}, t) + \mathcal{O}(\Delta t^3). \end{aligned} \quad (56)$$

The error analysis for this method has been carried out in [38–44]. The following will use eq. (55) since it is more efficient in section 4.5. With this approximation it is possible to make the kinetic energy operator diagonal in frequency space after a Fourier transform:

$$\mathcal{F}(T_{\mathbf{r}}) = \frac{\hbar^2}{2m}(2\pi\mathbf{f})^2, \quad (57)$$

$$\Rightarrow \mathcal{F}\left(\exp\left(-\frac{i}{\hbar}T_{\mathbf{r}}\frac{\Delta t}{2}\right)\right) = \exp\left(-\frac{i}{\hbar}\left(\frac{\hbar^2}{2m}(2\pi\mathbf{f})^2\right)\frac{\Delta t}{2}\right) \quad (58)$$

$$= \exp\left(-i\frac{\hbar}{2m}\frac{\Delta t}{2}(2\pi\mathbf{f})^2\right). \quad (59)$$

These split operators can be applied to  $\Psi(\mathbf{r}, t)$  by transforming it via the gdFT between position and frequency space in  $\mathcal{O}(N \log N)$  time before applying each operator. Therefore a full time step can be implemented with  $\mathcal{O}(N \log N)$  time complexity by transforming  $\Psi(\mathbf{r}, t)$  between the two spaces repeatedly:

$$\Psi_1(\mathbf{f}) = \Psi_0(\mathbf{f}) \exp\left(-i\frac{\hbar}{2m}\frac{\Delta t}{2}(2\pi\mathbf{f})^2\right), \quad (60)$$

$$\Psi_2(\mathbf{r}) = \widehat{\mathcal{F}}(\Psi_1(\mathbf{f})) \exp\left(-i\frac{1}{\hbar}\Delta t V(\mathbf{r}, t)\right), \quad (61)$$

$$\Psi_3(\mathbf{f}) = \mathcal{F}(\Psi_2(\mathbf{r})) \exp\left(-i\frac{\hbar}{2m}\frac{\Delta t}{2}(2\pi\mathbf{f})^2\right). \quad (62)$$

With FFTArray these formulas can be translated almost line by line into code to implement a single split-step Fourier time step of  $\Delta t$ :

```

1  from scipy.constants import hbar
2  import numpy as np
3  import fftarray as fa
```

```

4
5  def split_step(psi0: fa.Array, *,
6      dt: float,
7      mass: float,
8      V: fa.Array,
9      ) -> fa.Array:
10
11     k_sq = 0.
12     for dim in psi0.dims:
13         # Using coords_from_arr ensures that attributes
14         # like eager and xp do match the ones of psi.
15         k_sq = k_sq + (2*np.pi*fa.coords_from_arr(psi0, dim.name, "freq"))**2
16
17     psi1 = psi0.into_space("freq") * fa.exp((-1.j * hbar/(2*mass) * dt/2) * k_sq)
18     psi2 = psi1.into_space("pos") * fa.exp((-1.j * hbar * dt) * V)
19     psi3 = psi2.into_space("freq") * fa.exp((-1.j * hbar/(2*mass) * dt/2) * k_sq)
20
21     return psi3

```

The for-loop to compute  $k_{\text{sq}}$  and the automatic vectorization of arithmetic expressions enable this whole snippet to automatically support multiple dimensions and lazy evaluation (see section 3.3) automatically skips unnecessary phase factors. If  $\text{psi0}$  has `factors_applied` = `False`, the whole `split_step` routine never applies a single set of scale and phase factors, because each operator application is only a multiplication. Therefore, calling `split_step` multiple times in a loop does not have any per-step overhead while still supporting arbitrarily shifted coordinate grids. Every space change is just the call to `fft` or `ifft`, respectively. The `into_space` function allows the user to pass in  $\text{psi0}$  in any space and with any value for `factors_applied`. Any necessary transformations are done automatically. This and all following examples implement their calculations in SI units.

The split-step method can be modified to find the lowest energy eigenstate of an arbitrary potential. This so-called imaginary time evolution is achieved by replacing the time step  $\Delta t$  with an imaginary time step  $\Delta t \mapsto -i\Delta t$  such that the time evolution operator becomes  $\exp(-\frac{1}{\hbar}H(\mathbf{r}, t)\Delta t)$ . This causes each time step to dampen eigenstates with higher eigenenergies faster than the ones with lower energies. Since the whole wave function is dampened with every step, it would quickly become too small to be representable with the used floating point numbers. To prevent that it has to be renormalized after each time step.

We collected helper functions and definitions which are specific to quantum mechanical matter wave problems in a separate package called `matterwave` [45]. It contains an implementation of the split-step algorithm, often used constants and helper functions for normalizing wave functions and calculating expectation values and kinetic energies.

### 4.3 Bragg Diffraction of Matter Waves

In this example we solve the Schrödinger equation with the split-step method from section 4.2 to simulate matter wave diffraction in a Bragg grating made of light. Bragg diffraction is one of the central atom optical operations in atom interferometry [46, 47] to transfer several photon recoils of momentum without changing the internal state of the atoms [48–51]. This can be used to create a superposition of momentum states and thus is also referred to as a beam splitter. This example implements a semi-classical model of Bragg diffraction. The atom is described by a quantum-mechanical wave function. Due to its high enough intensity the light field is described classically since there are always enough photons [46, 52, 53]. Two counter-propagating laser beams form a lattice which causes elastic scattering of matter waves. This process does not change the internal state of the atom and the whole dynamics are described

with the following Hamiltonian [16]:

$$H(x, t) = -\frac{-\hbar^2}{2m} \frac{\partial^2}{\partial x^2} + 2\hbar\Omega(t) \cos^2(k_L x - 2\omega_r t) \quad (63)$$

where  $\Omega(t)$  is the time-dependent effective Rabi frequency.  $\Omega(t)$  is determined by the laser properties and is proportional to the intensity of the laser fields. The mass  $m$  in this example is for  $^{87}\text{Rb}$  and  $k_L$  is the wavenumber of the utilized atomic transition which is in this case the D2 line with a wavelength of 780 nm [54]. The single-photon recoil frequency of this wavelength is then  $\omega_r = \hbar k_L^2 / 2m$ . The initial state is defined to be a Gaussian with a momentum width of  $0.01\hbar k_L$ . The code reuses the `split_step` function of section 4.2 and the actual potential is simply the potential part of the Hamiltonian in eq. (63). Depending on the passed in ramp, this code simulates all Bragg regimes from Deep-Bragg to Raman-Nath as shown in [16].

```

1  import numpy as np
2  from scipy.constants import hbar
3
4  # Rb87 mass in kg
5  mass_rb87: float = 86.909 * 1.66053906660e-27
6  # Rb87 D2 transition wavelength in m
7  lambda_L: float = 780 * 1e-9
8  # Bragg beam wave vector
9  k_L: float = 2 * np.pi / lambda_L
10 hbar: float = hbar * k_L
11 # Single-Photon recoil frequency
12 w_r = hbar * k_L**2 / (2 * mass_rb87)
13
14 def simulate_bragg(t_arr, dt: float, rabi_frequency, ramp_arr, xp=np,
15 → dtype=np.float64):
16     # Returns the wave function after applying the Bragg beam potential to a
17     # Gaussian input state with 0.01 hbar k initial momentum width. The beam is
18     # assumed to be spatially homogeneous.
19     # t_arr: NumPy array containing the t of each time step.
20     # dt: Size of a time step
21     # rabi_frequency: Sets the magnitude of Ω(t), determined by the concretely
22     # used atom transition and laser detuning and intensity.
23     # ramp_arr: Scaling factor for Ω(t) for each time step.
24     # Ω(t) = rabi_frequency*ramp_arr
25
26
27     # Dimension for full sequence based on expected matter wave size and expansion
28     # → speed
29     dim_x: fa.Dimension = fa.dim_from_constraints("x",
30         pos_extent = 2e-3,
31         pos_middle = 0,
32         freq_middle = 0.,
33         freq_extent = 32. * k_L/(2*np.pi),
34         loose_params = ["freq_extent"])
35
36     # Initialize array with position coordinates.
37     x: fa.Array = fa.coords_from_dim(dim_x, "pos", xp=xp, dtype=dtype)
38
39     # Initialize harmonic oscillator ground state
40     sigma_p=0.01*hbar
41     psi: fa.Array = (2 * sigma_p**2 / (np.pi*hbar**2))**(.1./4.) *
42         fa.exp(-(sigma_p**2 / hbar**2) * x**2)
43     # Numerically normalize so that the norm is `1.` even though the tails of the
44     # → Gaussian are cut off.
45     psi *= fa.sqrt(1./fa.integrate(fa.abs(psi)**2))
46
47     # For each time step, compute the potential and evolve the wave function in it

```

```

41     for t, ramp in zip(t_arr, ramp_arr):
42         V = rabi_frequency * ramp * 2. * hbar * fa.cos(
43             k_L * x - 2. * w_r * t
44         )**2
45         psi: fa.Array = split_step(
46             psi,
47             dt=dt,
48             mass=mass_rb87,
49             V=V,
50         )
51
52     return psi

```

Depending on the specific scientific scenario, this implementation of Bragg diffraction might need different inputs and control parameters. Please note that different array libraries can require modifications to this code for peak performance, e.g. the JAX library requires to replace the above for loop with its `jax.lax.scan` function, see also section 5.

#### 4.3.1 Raman-Nath Regime

The Raman-Nath regime is characterized by a very short and bright pulse of a spatially symmetric beam splitter with a duration  $\tau \ll \frac{1}{\sqrt{2\Omega\omega_r}}$ . In this regime an analytical solution is available [46, 52]:

$$|g_n(t)|^2 = J_n^2(\Omega t) \quad (64)$$

where  $g_n(t)$  is the amplitude of the  $n$ -th momentum state  $|2n\hbar k\rangle$  and  $J_n$  the Bessel functions of first kind. Following [16], their demonstration scenario for this case with  $\Omega = 50\omega_r$  and  $\tau = 1\mu\text{s}$  with a rectangular intensity profile in time can be implemented with the code below.

```

1 rabi_frequency = 50*w_r
2 n_steps = 200
3 t_arr, dt = np.linspace(0., 1e-6, n_steps, retstep=True, endpoint=False)
4 ramp_arr = np.full(n_steps, 1.)
5
6 psi = simulate_bragg(t_arr, dt, rabi_frequency, ramp_arr)

```

The results of this code are visualized in fig. 4 and show very good agreement with the analytical solution.

#### 4.3.2 Bragg Regime

The laser intensity in a two-(momentum)-level beam splitter typically has a Gaussian temporal profile to ensure broad velocity selectivity such that most atoms participate in the Rabi oscillation between the two momentum states. The below code snippet implements a Gaussian temporal profile with  $\sigma = 25\text{ ms}$ , optimized to simulate a two-level single Bragg diffraction beam splitter in 401 steps. Special care was taken to sample the temporal profile symmetrically around  $t = 0$  while explicitly sampling the peak intensity.

```

1 # Use an odd number of steps to symmetrically sample the Gaussian
2 # and hit its peak at t=0 with a sample.
3 # Note that this snippet does not start at t=0 like above, but is symmetric around
4 # t=0.
5 n_steps = 401
6 # Rabi frequency. This specific value was found as a binary search to
# optimize a 50/50 split of the two momentum classes for this specific beam

```

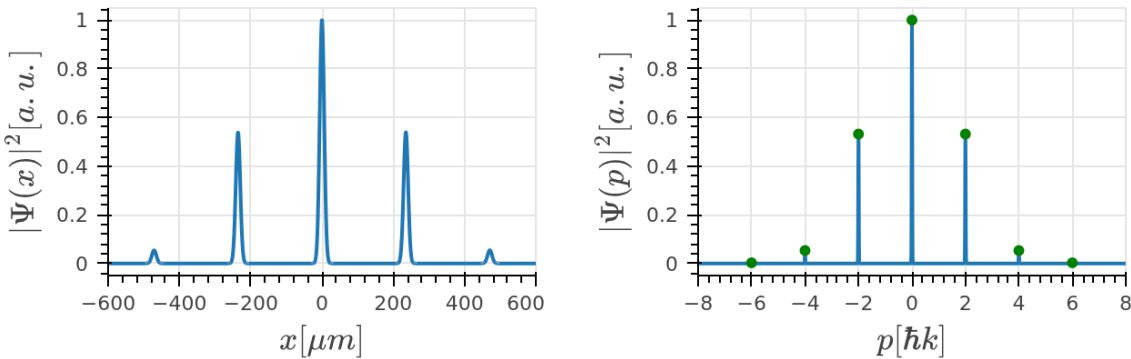


Figure 4: Probability density in position and momentum space after a Raman-Nath pulse with a rectangular temporal profile and  $\Omega = 50\omega_r$ ,  $\tau = 1\mu\text{s}$  followed by 20 ms of free propagation like in [16]. The green dots mark the analytical solution from eq. (64).

```

7  # splitter duration and pulse form.
8  rabi_frequency = 25144.285917282104 # Hz
9  sigma_bs = 25e-6 # temporal pulse width (s)
10 # The Gaussian is sampled from -4*sigma_bs to 4*sigma_bs
11 sampling_range_mult = 4.
12 t_arr, dt = np.linspace(
13     start=-sampling_range_mult*sigma_bs,
14     stop=sampling_range_mult*sigma_bs,
15     num=n_steps,
16     retstep=True,
17 )
18 # Gaussian density function
19 gauss = lambda t, sigma: np.exp(-0.5 * (t / sigma)**2)
20 # Remove the value of the Gauss at the beginning of the pulse so that
21 # the intensity starts and ends at zero.
22 gauss_offset = gauss(t = t_arr[0], sigma = sigma_bs)
23 ramp_arr = gauss(t = t_arr, sigma = sigma_bs) - gauss_offset
24
25 psi = simulate_bragg(t_arr, dt, rabi_frequency, ramp_arr)

```

The results of this beam splitter are visualized in fig. 5. It shows that the initial atom wave function with an average momentum of  $0\hbar k$  was split cleanly into a superposition of two momentum classes of  $0\hbar k$  and  $2\hbar k$ . The free propagation made this momentum split also visible in position space.

#### 4.4 Finding the Ground State of the Two-Dimensional Isotropic Quantum Harmonic Oscillator

The quantum harmonic oscillator is a central model system of quantum mechanics because it can be used to approximate many other systems. It is one of the few systems for which an exact, analytical solution for its eigenstates and eigenvectors is known. This makes it a very good opportunity to compare the numerical precision of a simple solver based on FFTArray with its exact solution. The isotropic quantum harmonic oscillator in  $n$  dimensions is defined as:

$$H = \frac{-\hbar^2 \nabla^2}{2m} + \frac{1}{2} m \omega^2 \mathbf{r}^2, \quad \mathbf{r} \in \mathbb{R}^n \quad (65)$$

In this case, the angular frequency  $\omega$  of the oscillator is the same in all directions.

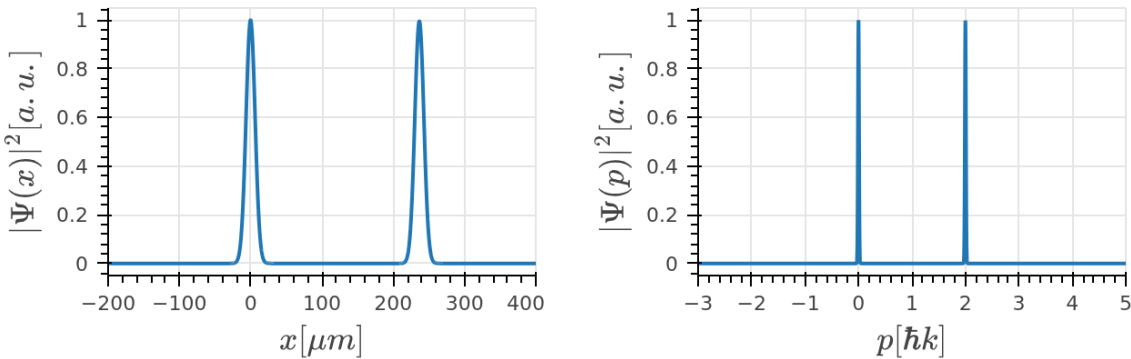


Figure 5: Probability density in position and momentum space of a Gaussian wave function with initial width of  $\Delta p = 0.01\hbar k$  after Bragg beam splitter with a  $\sigma = 25$  ms Gaussian temporal profile followed by 20 ms of free propagation. The 50/50 split between the two momentum classes  $|g, 0\rangle$  and  $|g, 2\hbar k_L\rangle$  works very well and these ideal parameters of long smooth pulses and very sharp peaks in momentum space do not yet show visible velocity selectivity.

The solution for its ground state energy is

$$E_0 = \hbar\omega \frac{n}{2}. \quad (66)$$

The following is a direct implementation of the imaginary time evolution described in section 4.2 for the isotropic quantum harmonic oscillator in two dimensions:

```

1 omega = 0.5*2.*np.pi
2
3 dim_x = fa.dim_from_constraints("x",
4     pos_min=-100e-6,
5     pos_max=100e-6,
6     freq_middle=0.,
7     n=2048,
8 )
9 y_dim = fa.dim_from_constraints("y",
10    pos_min=-100e-6,
11    pos_max=100e-6,
12    freq_middle=0.,
13    n=2048,
14 )
15
16 V: fa.Array = 0. # type: ignore
17 for dim in [dim_x, y_dim]:
18     V = V + 0.5 * mass_rb87 * omega**2. * fa.coords_from_dim(dim, "pos")**2
19
20 k_sq = 0.
21 for dim in [dim_x, y_dim]:
22     k_sq = k_sq + (2*np.pi*fa.coords_from_dim(dim, "freq"))**2
23
24 # Initialize psi as a constant function with value 1.
25 psi = fa.full(dim_x, "pos", 1.) * fa.full(y_dim, "pos", 1.)
26 for _ in range(n_steps):
27
28     psi = psi.into_space("pos") * fa.exp((-0.5 / hbar * dt) * V)
29     psi = psi.into_space("freq") * fa.exp((-1. * dt * hbar / (2*mass_rb87)) *
30         k_sq)
31     psi = psi.into_space("pos") * fa.exp((-0.5 / hbar * dt) * V)

```

```

32 state_norm = fa.integrate(fa.abs(psi)**2)
33 psi = psi * fa.sqrt(1./state_norm)

```

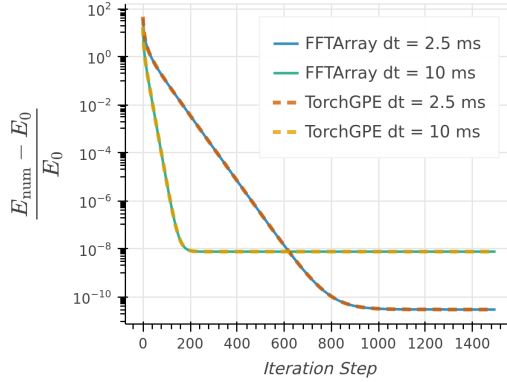


Figure 6: Absolute value of relative energy difference between the analytical and the numerical ground state of a 2D isotropic quantum harmonic oscillator for FFTArray and TorchGPE in float64. For both implementations, smaller time steps converge slower but are also able to more closely approach the analytic solution. With a time step of  $dt = 2.5$  ms both implementations reach the ground state energy with a relative error better than  $10^{-9}$ .

The energy of a wave function is the sum of its potential and kinetic energy:

$$E_{\text{tot}} = E_{\text{kin}} + E_{\text{pot}}, \quad (67)$$

$$E_{\text{kin}} = \frac{\hbar^2}{2m} \int d^n f |\Psi(f)|^2 (2\pi f)^2, \quad (68)$$

$$E_{\text{pot}} = \frac{\hbar^2}{2m} \int d^n r |\Psi(r)|^2 V(r). \quad (69)$$

As the metric for how well the found solution approximates the analytic solution we use the relative difference in energies between the numerical and analytical solution:

$$E_{\text{diff}} = \frac{E_{\text{num}} - E_0}{E_0} \quad (70)$$

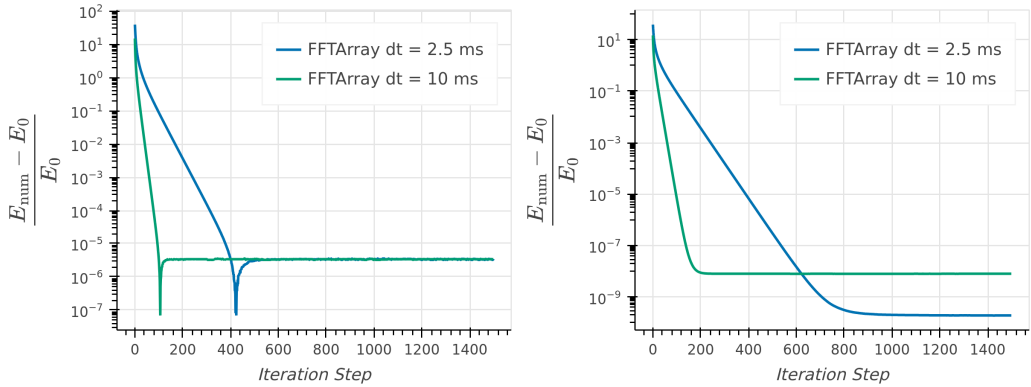
with  $E_{\text{num}}$  being the total energy of the numeric solution.

The resulting energies as a function of the number of time steps are shown in fig. 6. Smaller time steps converge slower but are able to reach the analytical solution more precisely. For reference we also added the results of an implementation with TorchGPE [11].

#### 4.4.1 Single Precision Simulation (float32)

The results in fig. 6 are computed with double precision (float64) numbers. However, there are only few use cases which require such high precision outside of scientific computing. Therefore, many GPUs feature much higher single precision than double precision compute or even just single precision compute. Examples for this are most current consumer GPUs like the NVIDIA AD102 (RTX 4090) which typically have 64 times more float32 compute than float64 compute [55].

Each algorithm and scenario potentially require a different numerical precision. As shown in fig. 7a, the precision of the result is reduced by about 4 orders of magnitude for  $dt = 2.5$  ms



(a) Imaginary time evolution and energy evaluation in float32. (b) Imaginary time evolution in float32 and energy evaluation in float64.

Figure 7: Relative energy difference between the analytical and the numerical ground state of a 2D isotropic quantum mechanic oscillator in single precision (float32) with FFTArray. On the left, the computation of the energy of the state is also done in float32 while on the right, only the imaginary time evolution is done in float32 while the energies are evaluated in float64. This hybrid approach shows an improvement of three orders of magnitude.

when doing the whole computation and evaluation in float32. The main limit in this case is not the actual imaginary time evolution but just the evaluation of the energy of the solution. When keeping the imaginary time evolution at float32 but computing the energy with float64 numbers, the precision is only reduced by about one order of magnitude compared to the float64 result. Implementing such hybrid algorithms is extremely easy with FFTArray because it only requires changing the data type of the `psi` array before passing it to the evaluation function.

#### 4.5 Finding a Two-Species Ground State in a Harmonic Trap

In this example, we perform an imaginary time evolution to find the ground state of two interacting atomic species within harmonic potentials. In particular, we describe a system of two magnetically trapped Bose Einstein condensates (BECs) of  $^{87}\text{Rb}$  and  $^{41}\text{K}$ , relevant in fundamental physics experiments [56,57]. The traps can be described with three-dimensional anisotropic harmonic potentials with different trap frequencies for each of the two species. Typically, these form a cigar shape with two large frequencies in two dimensions and one small frequency in the third dimension.

We describe this quantum mechanical system via a coupled Gross-Pitaevskii equation (GPE). The GPE of a single species is a non-linear Schrödinger equation with a term that describes the self-interaction of the atoms. It is quantified by the scattering amplitudes  $g_{\text{Rb}}$  and  $g_{\text{K}}$ , respectively. The coupled GPE additionally features an additional interaction between the two different species with the scattering amplitude  $g_{\text{Rb},\text{K}}$ . The respective time-independent Hamiltonians for these wavefunctions are [15,58]:

$$H_{\text{Rb}}(\mathbf{r}, t) = -\frac{\hbar^2}{2m_{\text{Rb}}} \nabla_{\mathbf{r}}^2 + V_{\text{Rb}}^{\text{ext}}(\mathbf{r}) + N_{\text{Rb}} g_{\text{Rb}} |\Psi_{\text{Rb}}(\mathbf{r})|^2 + N_{\text{K}} g_{\text{Rb},\text{K}} |\Psi_{\text{K}}(\mathbf{r})|^2, \quad (71)$$

$$H_{\text{K}}(\mathbf{r}, t) = -\frac{\hbar^2}{2m_{\text{K}}} \nabla_{\mathbf{r}}^2 + V_{\text{K}}^{\text{ext}}(\mathbf{r}) + N_{\text{K}} g_{\text{K}} |\Psi_{\text{K}}(\mathbf{r})|^2 + N_{\text{Rb}} g_{\text{Rb},\text{K}} |\Psi_{\text{Rb}}(\mathbf{r})|^2, \quad (72)$$

with the respective number of atoms in the BEC  $N_{\text{Rb},\text{K}}$ , the atom mass  $m_{\text{Rb},\text{K}}$  and a 3-dimensional anisotropic trapping potential  $V_{\text{Rb},\text{K}}^{\text{ext}}$  like in section 4.4 with a frequency relation

$$\omega_K^i = (m_{\text{Rb}}/m_K)^{1/2} \omega_{\text{Rb}}^i.$$

Performing the imaginary time evolution for two coupled wave functions instead of a single one can be straightforwardly implemented by adapting 4.2. The total potential  $V(\mathbf{r}, t)$  can be written directly as a sum of the external potential, the self-interaction and the interaction with the other species. This is possible as FFTArray offers full control over each time step while both, wave functions and operators, are free-standing Array objects which can be combined arbitrarily. The following shows a single imaginary time step of the above system:

```

1  def imaginary_time_step_dual_species(
2      psi_rb87: fa.Array,
3      psi_k41: fa.Array,
4      rb_potential: fa.Array,
5      k_potential: fa.Array,
6      dt: float,
7  ) -> Tuple[fa.Array, fa.Array]:
8      """
9          Perform a single imaginary time step for the dual species GPE.
10         """
11
12         ## Calculate the potential energy operators (used for split-step and plots)
13         psi_rb87 = psi_rb87.into_space("pos")
14         psi_k41 = psi_k41.into_space("pos")
15
16         psi_pos_sq_rb87 = fa.abs(psi_rb87)**2
17         psi_pos_sq_k41 = fa.abs(psi_k41)**2
18
19         self_interaction_rb87 = num_atoms_rb87 * coupling_rb87 * psi_pos_sq_rb87
20         interaction_rb87_k41 = num_atoms_k41 * coupling_rb87_k41 * psi_pos_sq_k41
21         V_rb87 = self_interaction_rb87 + interaction_rb87_k41 + rb_potential
22
23         self_interaction_k41 = num_atoms_k41 * coupling_k41 * psi_pos_sq_k41
24         interaction_k41_rb87 = num_atoms_rb87 * coupling_rb87_k41 * psi_pos_sq_rb87
25         V_k41 = self_interaction_k41 + interaction_k41_rb87 + k_potential
26
27         ## Imaginary time split step application
28
29         psi_rb87 = split_step_imaginary_time(
30             psi=psi_rb87,
31             V=V_rb87,
32             dt=dt,
33             mass=m_rb87,
34         )
35         psi_k41 = split_step_imaginary_time(
36             psi=psi_k41,
37             V=V_k41,
38             dt=dt,
39             mass=m_k41,
40         )
41
42         return psi_rb87, psi_k41

```

```

1  import jax.numpy as jnp
2  from functools import reduce
3
4  def split_step_imaginary_time(
5      psi: fa.Array,
6      V: fa.Array,
7      dt: float,
8      mass: float,
9  ) -> fa.Array:

```

```

10     """Perform an imaginary time split-step of second order in VPV
11     → configuration."""
12
13     # Calculate half step imaginary time potential propagator
14     V_prop = fa.exp((-0.5*dt / hbar) * V)
15     # Calculate full step imaginary time kinetic propagator (k_sq = kx^2 + ky^2 +
16     → kz^2)
17     k_sq = reduce(lambda a,b: a+b, [
18         (2*np.pi * fa.coords_from_dim(dim, "freq", xp=jnp, dtype=jnp.float64))**2
19         for dim in psi.dims
20     ])
21     T_prop = fa.exp(-dt * hbar * k_sq / (2*mass))
22
23     # Apply half potential propagator
24     psi = V_prop * psi.into_space("pos")
25
26     # Apply full kinetic propagator
27     psi = T_prop * psi.into_space("freq")
28
29     # Apply half potential propagator
30     psi = V_prop * psi.into_space("pos")
31
32     # Normalize after step
33     state_norm = fa.integrate(fa.abs(psi)**2)
34     psi = psi / fa.sqrt(state_norm)

     return psi

```

For the full code including the initialization of all functions and constants including energy tracking, we refer to the corresponding example in the repository [59]. Figure 8 shows the final probability densities for both species. They qualitatively match the results shown in [15] from where we adopted the system parameters.

Note that in this case it is beneficial to split the operator with two times the potential as in eq. (55). The potential has to be computed before applying the first of the split operators, in order to not degrade into an effectively first order propagation. With the above split (eq. (55)) of the evolution operator, the wave functions are already in position space before and after each time step which allows to directly compute the self-interaction from it. With the other split as in eq. (56), they would be in frequency space before a time step and the potential calculation would require the execution of two additional IFFTs per time step.

## 5 Computational Performance Evaluation

In the following, we evaluate the computational performance of FFTArray on one of our previous examples. We compare the array libraries NumPy and JAX as well as the execution on different hardware. Due to the breadth of possible implementations on top of FFTArray, any performance evaluation can only look at a small subset of possible scenarios. This section uses as an example the imaginary time evolution from section 4.4.

This section evaluates whether FFTArray maintains performance comparable to directly using the underlying array library's FFT methods. The comparison focuses on large domains and a split-step algorithm with many time steps since those are for us the most performance-limited scenarios. In order to focus on those, we exclude startup and initialization costs from the time measurement as much as possible. In order to extract the run-time per step and remove any remaining startup costs, we perform a linear fit of the results for three different numbers of time steps and take the fitted slope as our result in computational time per time

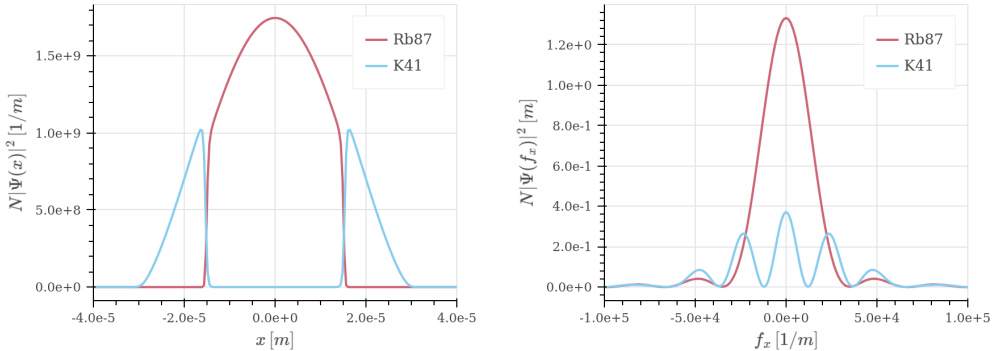


Figure 8: The computed ground state probability densities of the  $^{87}\text{Rb}$  and  $^{41}\text{K}$  BECs normalized to the number of atoms per species, shown in both position and frequency space. The repelling force between the two species splits up  $^{41}\text{K}$  along the weak trapping axis  $x$ . The plotted position and frequency space regions are zoomed in with respect to the actual domain sizes.

step. For more details on all these reduction steps see section A.2 and section A.3.

We compare three different implementations of the same imaginary time evolution. They all execute the exact same algorithm but organize the computations differently. The first one is the code from section 4.4 which will be labeled as "FFTArray Direct".

The potential and time step  $dt$  are the same for each step in this scenario. We can thus compute the propagators once before the loop and then reuse them at each step. This insight yields the second implementation which is called "FFTArray Precomputed":

```

1 # <Same initialization as in the original example.>
2
3 V = get_V(psi)
4 k_sq = 0.
5 for dim in psi.dims:
6     # Using coords_from_arr ensures that attributes
7     # like eager and xp do match the ones of psi.
8     k_sq = k_sq + (2*np.pi*fa.coords_from_arr(psi, dim.name, "freq"))**2
9
10 T_prop = fa.exp((-1. * dt * hbar / (2*mass)) * k_sq)
11 V_prop = fa.exp((-0.5 / hbar * dt) * V)
12
13 for _ in range(n_steps):
14     psi = psi.into_space("pos") * V_prop
15     psi = psi.into_space("freq") * T_prop
16     psi = psi.into_space("pos") * V_prop
17
18     state_norm = fa.integrate(fa.abs(psi)**2)
19     psi = psi * fa.sqrt(1./state_norm)

```

In order to measure how much overhead FFTArray causes inside the loop, we create a a third benchmark variant which does not use any code of FFTArray inside the loop and is called "Raw FFT":

```

1 # <Same initialization as in the above example.>
2
3 T_prop = fa.exp((-1. * dt * hbar / (2*mass)) * k_sq)
4 V_prop = fa.exp((-0.5 / hbar * dt) * V)
5

```

```

6  T_prop_arr = T_prop.values("freq")
7  V_prop_arr = V_prop.values("pos")
8  # Need the raw inner values, which are not accessible via a public API
9  # Using these inner values allows us to use the whole infrastructure and phase
10 # In the inner loop below FFTArray would not need to apply any phase and scale
11 # factors because they would cancel out.
12 psi = psi.into_space("pos").into_factors_applied(False).values
13
14 for _ in range(n_steps):
15     psi *= V_prop_arr
16     psi = xp.fft.fftn(psi)
17     psi *= T_prop_arr
18     psi = xp.fft.ifftn(psi)
19     psi *= V_prop_arr
20
21     state_norm = xp.sum(xp.abs(psi)**2)*vol_elem
22     psi *= xp.sqrt(1./state_norm)
23
24     # Repack the raw values correctly.
25     # Again there is no public API for that.
26     psi = fa.array(values, [x_dim, y_dim], "pos")
27     psi._factors_applied = (False,)*len(dims)

```

This manually eliminates FFTArray completely from the inner loop in order to test whether the book-keeping of FFTArray creates measurable overhead when ensuring dimensions line up and phase factors are applied if necessary. Doing something like this in practice also abandons the advantages FFTArray offers, which is why this code snippet needs to access private implementation details of FFTArray.

These three implementations are measured with two different array libraries. NumPy is the base reference and only runs on CPUs. For GPU support and potentially less overhead on CPUs, we use the JAX library. They recommend using special structured control flow primitives [60] in order to achieve best performance. Therefore, the `for` loop is replaced with `jax.lax.scan` for these measurements. This ensures that JAX can optimize the whole loop as one unit and operations are potentially fused which can increase performance and reduce the per-step overhead.

In order to give a broad overview of the implementations on different hardware, we chose one server and one desktop CPU (AMD Epyc 7543, AMD Ryzen 7950X3D) and GPU (NVIDIA A100, NVIDIA RTX 4090) respectively, for more details see section A.1.

These measurements were done at a resolution of 4096 by 4096 samples such that the values reflect the speed in the limit of large wave functions as well as possible. With this number of samples, the complex-valued wave function has a size of 128 MiB (float32) and 256 MiB (float64), respectively, which does not fit in any of the caches of the tested processors. Other domain sizes can be estimated roughly by linearly extrapolating, for details to the scaling as a function of domain size and shape, see section A.4.

The results in fig. 9 show the extremely large performance difference between CPUs and GPUs for this example. The JAX implementation is about two orders of magnitude faster in most cases on the two GPUs compared to the two CPUs. This shows that it is worthwhile to use the consumer GPUs over any kind of CPUs even if the computations have to happen in float64.

The tracing and batching of the `scan`-function of JAX is able to achieve almost the same speed in all three implementations on both CPUs and GPUs. It therefore shows that FFTArray does not add any measurable overhead compared to using the underlying array library directly for large arrays and time steps. This means, when using JAX, users can even take advantage of the comfort of directly writing down the formulas without a significant hit to performance

on any of the tested platforms.

The NumPy implementation only runs on the CPUs and is slower than JAX on the same hardware. "FFTArray Direct" is significantly slower than the other two implementations. This is expected since NumPy cannot fuse multiple operations together which causes a much higher memory overhead for recomputing the propagators at each time step. However, when pre-computing the propagators in "FFTArray Precomputed" the overhead for managing dimensions and phase factors becomes small in the tested scenario and this implementation achieves comparable speeds to the "Raw FFT" variant. Therefore, our goal of not introducing overhead for our key use-cases is also achieved with NumPy.

The A100 is faster than the RTX 4090 in float64 while it is the other way around in float32. This difference is less pronounced than their huge differences in peak compute performance would suggest. Performance is most likely bound more by memory accesses than raw compute performance in many parts of the algorithm.

In order to give a comparison to an existing state-of-the-art solution, measurement results of TorchGPE are listed at the bottom of the chart for the same hardware. The resolution in position space is the same as in the FFTArray implementation. However, it uses twice as many samples in frequency space to reduce boundary effects [61]. As shown in fig. 6 this does not yield a significantly better precision in this scenario. Since this feature cannot be deactivated at the time of writing, it is part of the overhead of TorchGPE in this scenario. Even if its performance was a factor of two better, our solution is still multiple times faster in the measured scenario.

## 6 Conclusion and Outlook

FFTArray introduces a framework for implementing discretized Fourier transforms on arbitrarily shifted coordinate grids. It enables researchers to translate Fourier integral formulas directly into code and easily scales from single to multiple dimensions via named dimensions. Numerical details like choosing valid coordinate grids and implementing all necessary phase and scale factors to obtain a discretized Fourier transform are handled automatically without performance overhead for large simulations. By being built upon the Python Array API standard, FFTArray enables high performance on GPUs that reduces simulation run times significantly and makes large-scale 3D simulations computationally feasible. This was already utilized successfully with in-development versions of FFTArray for multiple scientific publications [62–65].

FFTArray allows researchers to focus on the core scientific challenges rather than the intricacies of Fourier transform implementations, therefore enabling the rapid prototyping of complex models.

Many of the library's central ideas like its constraint solver, the encapsulation of coordinates per dimension and giving the user explicit but automated control over phase and scale factor applications are language-independent and may be adapted to other programming languages. We hope that FFTArray's modular architecture and design will empower researchers to tackle Fourier-related challenges more effectively. Furthermore, we invite the scientific community to expand upon our existing implementations, such as our matter wave simulation package [45], as well as to contribute to this package and build new solvers on top it.

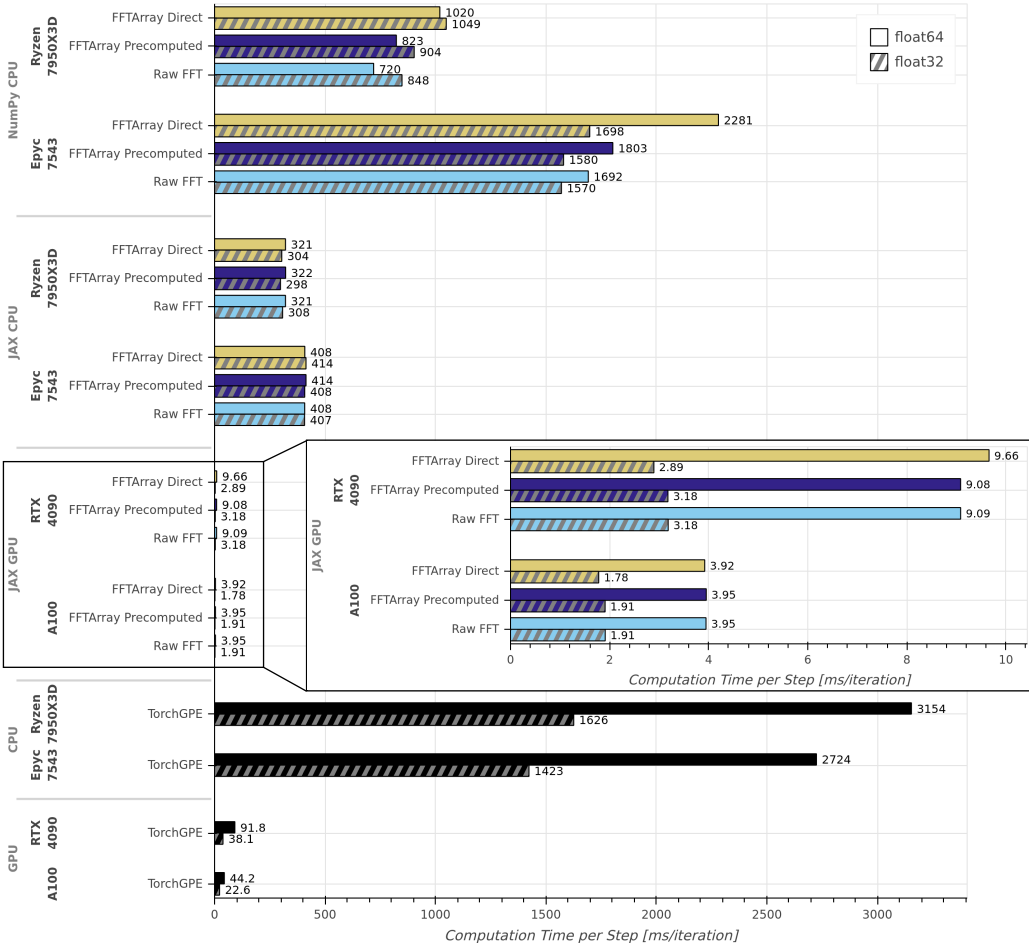


Figure 9: Computation time per time step on the problem of finding the ground state of an isotropic 2D quantum harmonic oscillator. This compares different loop implementations and hardware at a resolution of 4096 by 4096 samples. The similar performance between "Raw FFT" and "FFTArray Precomputed" demonstrates that FFTArray introduces negligible overhead. GPUs are about two orders of magnitude faster than CPUs and should therefore be preferred in most cases. The comparison with TorchGPE shows that the performance of this implementation is better than other state-of-the-art solutions in this scenario.

**Code Availability** The code of FFTArray is openly available at <https://github.com/QSTheory/fftarray> and our matter wave specific library is openly available at <https://github.com/QSTheory/matterwave>, both under Apache-2.0 license.

## Acknowledgements

We thank our science group for feedback on earlier versions of this package and helping us charting out the variety of use cases for this package. S.J.S. thanks Florian Fitzek for his introduction, guidance and Fortran codes for the simulation of matter wave interferometers. We thank Eric Charron for his feedback on an intermediate version of the library. S.J.S. thanks Alexander Hahn for discussions, guidance about Trotter product formulas and split-step algorithms and very helpful feedback to a draft of this paper. G.M. thanks Annie Pichery for discussions about the two species ground state example. S.J.S. thanks Michael Werner for his help and comments about the mathematical foundations of the Fourier Transform.

**Funding information** This work was funded by the Deutsche Forschungsgemeinschaft (German Research Foundation) under Germany's Excellence Strategy (EXC-2123 QuantumFrontiers Grants No. 390837967), through CRC 1227 (DQ-mat) within Projects No. A05 and the German Space Agency (DLR) with funds provided by the German Federal Ministry for Economic Affairs and Climate Action (BMWKG) (German Federal Ministry of Education and Research (BMBF)) due to an enactment of the German Bundestag under Grants No. 50WM2245A (CAL-II), No. 50WM2263A (CARIOQA-GE) and No. 50WM2253A (AI-Quadrat). NG acknowledges funding by the AGAPES project - grant No 530096754 within the ANR-DFG 2023 Programme. J.-N. K.-S., G.M., C.S. and S.J.S. acknowledge support from QuantumFrontiers through the QuantumFrontiers Entrepreneur Excellence Programme (QuEEP). J.-N. K.-S., G.M., S.J.S. and N.G. acknowledge funding from the EU project CARIOQA-PMP (101081775).

## A Computation Speed as a Function of Time Steps and Function Samples

This section describes in more detail the methods, hardware and software used to create the speed measurements in section 5. In order to generate the numbers shown in fig. 9, a few assumptions about the distribution of our measurement data were made, like the linearity of simulation time as a function of time steps. These are also described and justified in this section.

The measured simulation is an imaginary time evolution to find the ground state of an n-dimensional harmonic oscillator as described in sections 4.2 and 4.4. This means that among others, there are the following numerical parameters:

- The number of iterations, i.e., imaginary time steps.
- The number of samples to discretize each of the up to three dimensions.
- The precision of the used floating point numbers to represent a sample. We used float32 and float64.

### A.1 Hardware Selection and System Details

The measurements for computation speed were done on one server and one desktop computer.

The server is a dual-socket Dell PowerEdge R7525. The two CPUs are AMD Epyc 7543 with 32 Zen 3 cores with eight DDR4-3200 memory channels each. The measurements were limited to one of the CPUs which was configured as a single NUMA node. This sever also contains three NVIDIA A100 80GiB PCIe cards, with one of those used for the measurements. The A100 is a server GPU which was specifically designed for high performance scientific computing and machine learning. It features a peak memory bandwidth of up to 1.94 TB/s and a 1:2 ratio between float32 (19.5 TFLOPS) and float64 (9.7 TFLOPS) performance [66].

The desktop computer consists of an AMD Ryzen 7950X3D CPU and an NVIDIA RTX 4090. The CPU is a high-end desktop CPU with 16 Zen 4 cores and two memory channels of DDR5-5200 RAM. The 16 cores are split into two chiplets with 8 cores each. One chiplet has an additional X3D-Cache which increases its local L3 cache to 96 MiB. The Nvidia RTX 4090 is a high-end consumer GPU. This means it is easier and cheaper to procure and can be used in a normal desktop whereas the A100 is only available for servers. It features also relatively high memory bandwidth (1008 GB/s) but since its focus are graphics workloads, it only has a 1:64 ratio of float64 (1.29 TFLOPS) to float32 (82.6 TFLOPS) performance [55].

Both systems were running Ubuntu 24.04.2 LTS with the NVIDIA driver 570.133.07 and CUDA 12.8. The versions of the used array libraries were NumPy 2.2.6, JAX 0.6.1 and PyTorch 2.7.0. The used version of TorchGPE was the latest public version as of 11 July 2025, c02428f on <https://github.com/qo-eth/TorchGPE>.

## A.2 Measurement Methodology

In order to isolate the computational speed in the limit of many time steps, the following procedure was used: First, the simulation is run twice with two time steps in each run as a warm-up to reduce effects due to module imports, compilation caches and other initialization routines which depend on the specific system configuration and software versions.

We only time the inner loop of the simulation without any initialization or clean-up routines while ensuring that after the simulation, the computation results from the GPU have been sent back to the CPU. To reduce run-to-run variations due to interference by other processes, each measurement was done four times and the minimum measured time was taken. This assumes that there is a best case speed and any runtime variation is caused by interruptions which ideally do not happen. To eliminate any startup costs, we use the fact that the simulation time scales linearly in the number of time steps (section A.3). For each point in figs. 9 and 11 to 13, we measure for three different numbers of time steps. The base number of steps is adjusted via a calibration run such that the simulation loop takes about ten seconds, the other two time step groups are then two and four times as many time steps which results in a targeted runtime of 20 and 40 seconds, respectively. Each of the points in the diagram figs. 9 and 11 to 13 is then the slope of a linear fit through the minimum runtime for each of the three different numbers of time steps.

## A.3 Scaling in the Number of Time Steps

Theoretically the run time should increase linearly as a function of the number of time steps. As shown in fig. 10 this is indeed the case for the "FFTArray Direct" variant and TorchGPE. Each plot also visualizes the run-to-run variation by plotting all slower runs as grey markers. In most cases, these are not even visible. The points, reduced via taking the minimum, show a clear linear scaling in the number of time steps as shown by the linear fits.

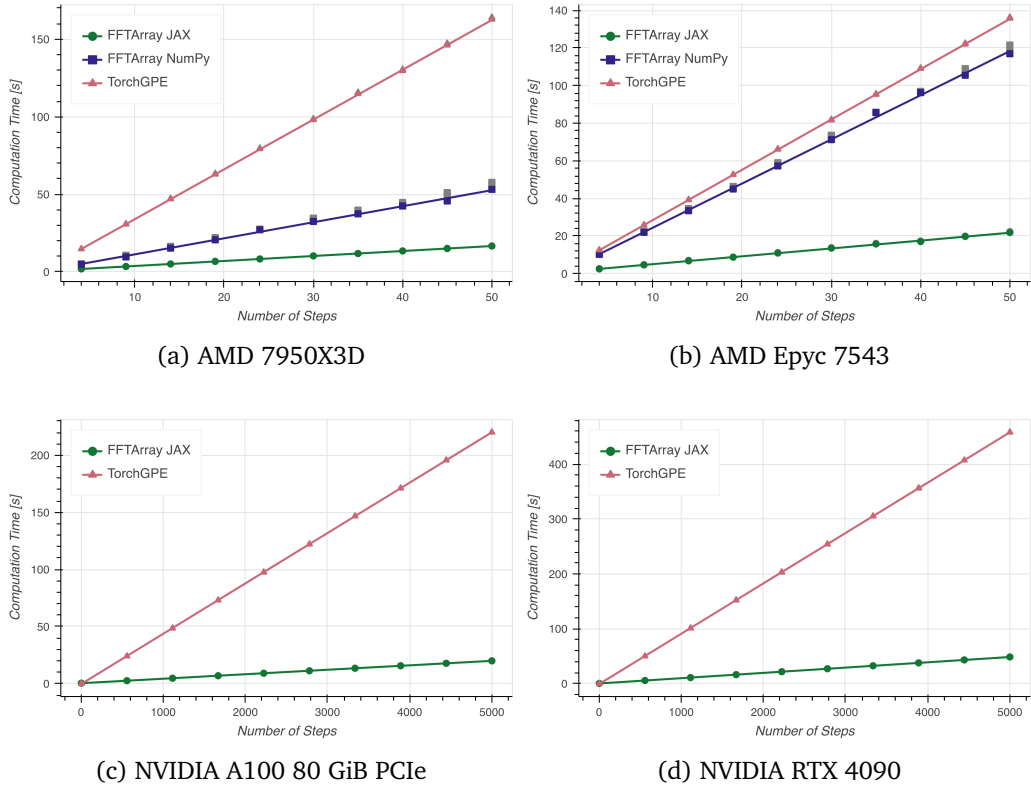


Figure 10: The measured run time for an imaginary time evolution of 4096 by 4096 samples in an isotropic harmonic potential as a function of the number of time steps in float64 precision. The used implementations are "FFTArray Direct" for the FFTArray cases and TorchGPE. Grey markers show the durations of the runs which were not selected by the minimum reduction. On most points all measurements are so close together that they overlap with the selected point and are not visible. The lines are linear fits on the minimum run time for each duration. All implementations on all hardware configurations show a clear linear scaling in the number of steps which is also the expected behavior.

#### A.4 Scaling in the Number of Samples and Shape of the Domain

The time complexity class of the simulation algorithm as a function of samples is  $\mathcal{O}(n_{\text{samples}} \log n_{\text{samples}})$  for the number of samples in each dimension. This comes from the fact that this is the complexity class of the FFT while all other operations are in the class  $\mathcal{O}(n_{\text{samples}})$ . However, in practice other factors can be more dominant. There is for example a whole hierarchy of memory types with different speed and size. The fastest and smallest are the registers, then there are two to three levels of caches and then the (V)RAM. Additionally, not all memory accesses are equal, since most processors always have to load data at a minimum granularity. Therefore the data layout and the memory access patterns of algorithms can have a huge impact on performance. To get a rough overview of how important these factors are, the "FFTArray Direct" and TorchGPE implementations were tested for different grid sizes and layouts. We always compare the same total number of samples, but these samples are distributed into different shapes:

- 1D: The domain is a single dimension which contains all samples.
- 2D: The domain is two-dimensional with both sides having the same number of samples.
- 3D: The domain is three-dimensional with all three sides having the same number of samples.
- (64, 64, nz): The first and second dimension have 64 samples while the z dimension has a number of samples which is a power of two. This scenario is for example relevant for the case of a Bragg beam splitter. The Bragg beam splitting process requires a higher resolution in the beam direction than the other directions.
- (nx, 64, 64): This is in principle the same shape as the case before. But due to the different ordering of axes, this may change the memory access patterns of the algorithm. This case is tested to see if that makes a significant difference.

In order to always test the exact same FFT algorithm, each axis must have a size which is a power of two. Notably, that means that for example the 3D case can only be tested for a total number of samples of  $2^{3n}$  with  $n$  being a natural number. Additionally we only tested starting from a minimum size of 64 samples per axis and a total minimum number of samples of  $2^{20}$  for FFTArray and  $2^{18}$  for TorchGPE, since smaller numbers are not that interesting for our applications. TorchGPE only officially supports 2D, so only that shape was tested.

The measurements in this section were done according to section A.2 including a linear fit over multiple runs with different numbers of steps.

The results for JAX (fig. 11) and TorchGPE (fig. 13) show a mostly linear scaling for all hardware devices while NumPy (fig. 12) shows a worse than linear scaling, especially in the 1D case. The approximately linear scaling despite the theoretical complexity class of  $\mathcal{O}(n_{\text{samples}} \log n_{\text{samples}})$  shows that we are apparently still in a regime of  $n_{\text{samples}}$  where other factors dominate the run time. With the exception of the 1D case on CPUs, all layouts show a similar performance, so a good estimation of computational speed can be done simply from the number of samples and time steps. Notably, the 1D case is slower than the other layouts on CPU with both the NumPy and the JAX implementation but on the GPUs all layouts are comparable.

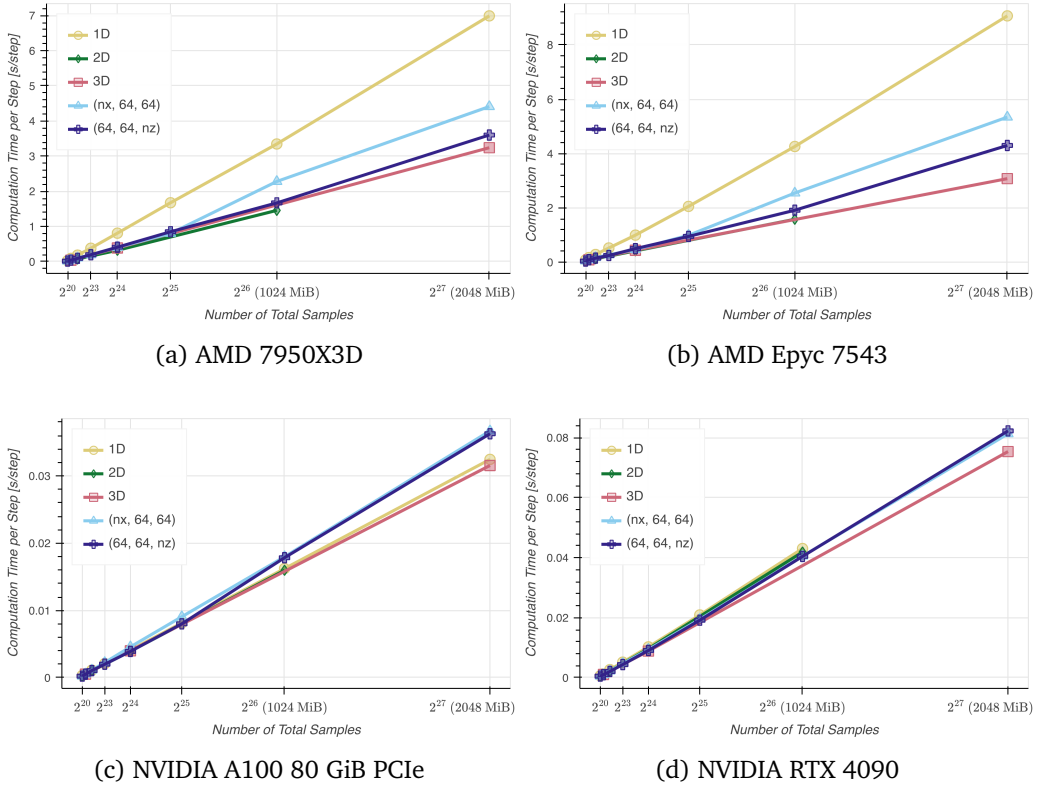


Figure 11: Computation time per step as a function of the number of samples and their layout with the JAX "FFTArray Direct" implementation in float64. Even though the theoretical scaling is  $\mathcal{O}(n_{\text{samples}} \log n_{\text{samples}})$ , JAX effectively scales linearly in the number of samples. All layouts are reach similar speeds with the exception of the 1D case on CPUs which is significantly slower. On GPUs the 1D case also achieves similar speeds to the other layouts. All points are directly connected for better visual clarity.

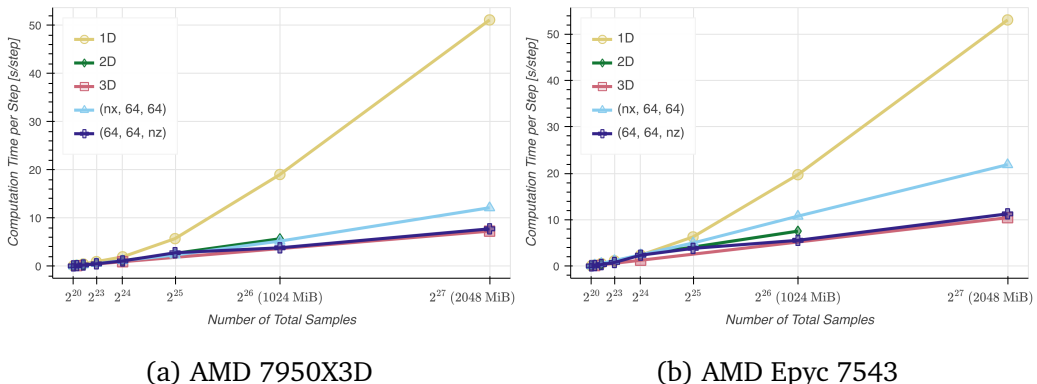


Figure 12: Computation time per step as a function of the number of samples and their layout with the NumPy "FFTArray Direct" implementation in float64. NumPy shows a slower than linear scaling in the number of samples. All layouts are simulated at similar speeds with the exception of the 1D case which is significantly slower. All points are directly connected for better visual clarity.

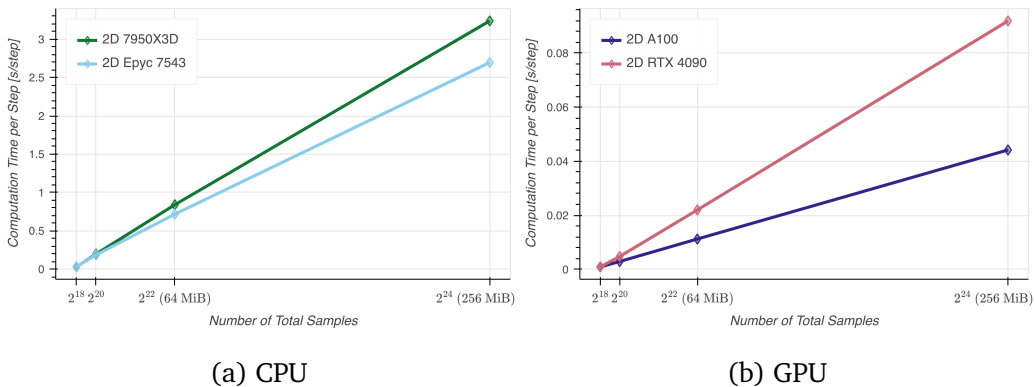


Figure 13: Computation time per step as a function of the number of samples and their layout with the TorchGPE implementation in float64. Even though the theoretical scaling is  $\mathcal{O}(n_{\text{samples}} \log n_{\text{samples}})$ , TorchGPE effectively scales linearly in the number of samples. Only the 2D configuration was tested since TorchGPE does not support 1D or 3D domains. All points are directly connected for better visual clarity.

## References

- [1] M. J. Feit, J. A. Fleck and A. Steiger, *Solution of the Schrödinger equation by a spectral method*, *Journal of Computational Physics* **47**, 412 (1982), doi:[10.1016/0021-9991\(82\)90091-2](https://doi.org/10.1016/0021-9991(82)90091-2).
- [2] E. Hairer, G. Wanner and C. Lubich, *Geometric Numerical Integration*, vol. 31 of *Springer Series in Computational Mathematics*, Springer Berlin Heidelberg, Berlin, Heidelberg, ISBN 978-3-662-05020-0 978-3-662-05018-7, doi:[10.1007/978-3-662-05018-7](https://doi.org/10.1007/978-3-662-05018-7) (2002).
- [3] C. Shannon, *Communication in the Presence of Noise*, *Proceedings of the IRE* **37**(1), 10 (1949), doi:[10.1109/JRPROC.1949.232969](https://doi.org/10.1109/JRPROC.1949.232969).
- [4] C. R. Harris, K. J. Millman, S. J. van der Walt, R. Gommers, P. Virtanen, D. Cournapeau, E. Wieser, J. Taylor, S. Berg, N. J. Smith, R. Kern, M. Picus *et al.*, *Array programming with NumPy*, *Nature* **585**(7825), 357 (2020), doi:[10.1038/s41586-020-2649-2](https://doi.org/10.1038/s41586-020-2649-2).
- [5] J. Bradbury, R. Frostig, P. Hawkins, M. J. Johnson, C. Leary, D. Maclaurin, G. Necula, A. Paszke, J. VanderPlas, S. Wanderman-Milne and Q. Zhang, *JAX: composable transformations of Python+NumPy programs*, <https://github.com/google/jax>, Version 0.6.1 (2018).
- [6] J. Ansel, E. Yang, H. He, N. Gimelshein, A. Jain, M. Voznesensky, B. Bao, P. Bell, D. Beillard, E. Burovski, G. Chauhan, A. Chourdia *et al.*, *PyTorch 2: Faster machine learning through dynamic python bytecode transformation and graph compilation*, In *29th ACM International Conference on Architectural Support for Programming Languages and Operating Systems, Volume 2 (ASPLOS '24)*. ACM, doi:[10.1145/3620665.3640366](https://doi.org/10.1145/3620665.3640366) (2024).
- [7] X. Antoine and R. Duboscq, *GPELab, a Matlab toolbox to solve Gross–Pitaevskii equations I: Computation of stationary solutions*, *Computer Physics Communications* **185**(11), 2969 (2014), doi:[10.1016/j.cpc.2014.06.026](https://doi.org/10.1016/j.cpc.2014.06.026).
- [8] X. Antoine and R. Duboscq, *GPELab, a Matlab toolbox to solve Gross–Pitaevskii equations II: Dynamics and stochastic simulations*, *Computer Physics Communications* **193**, 95 (2015), doi:[10.1016/j.cpc.2015.03.012](https://doi.org/10.1016/j.cpc.2015.03.012).

[9] J. Schloss and L. O'Riordan, *GPUE: Graphics Processing Unit Gross–Pitaevskii Equation solver*, Journal of Open Source Software **3**(32), 1037 (2018), doi:[10.21105/joss.01037](https://doi.org/10.21105/joss.01037).

[10] B. D. Smith, L. W. Cooke and L. J. LeBlanc, *GPU-accelerated solutions of the nonlinear Schrödinger equation for simulating 2D spinor BECs*, Computer Physics Communications **275**, 108314 (2022), doi:[10.1016/j.cpc.2022.108314](https://doi.org/10.1016/j.cpc.2022.108314).

[11] L. Fioroni, L. Gravina, J. Stefaniak, A. Baumgärtner, F. Finger, D. Dreon and T. Donner, *A Python GPU-accelerated solver for the Gross-Pitaevskii equation and applications to many-body cavity QED*, SciPost Physics Codebases p. 38 (2024), doi:[10.21468/SciPostPhysCodeb.38](https://doi.org/10.21468/SciPostPhysCodeb.38).

[12] C. J. Pethick and H. Smith, *Bose–Einstein Condensation in Dilute Gases*, Cambridge University Press, 2 edn., ISBN 978-0-521-84651-6 978-0-511-80285-0, doi:[10.1017/cbo9780511802850](https://doi.org/10.1017/cbo9780511802850) (2008).

[13] E. P. Gross, *Hydrodynamics of a superfluid condensate*, Journal of Mathematical Physics **4**(2), 195 (1963), doi:[10.1063/1.1703944](https://doi.org/10.1063/1.1703944).

[14] L. P. Pitaevskii, *Vortex lines in an imperfect Bose gas*, Soviet Physics–JETP [translation of Zhurnal Eksperimentalnoi i Teoreticheskoi Fiziki] **13**(2), 451 (1961).

[15] A. Pichery, M. Meister, B. Piest, J. Böhm, E. M. Rasel, E. Charron and N. Gaaloul, *Efficient numerical description of the dynamics of interacting multispecies quantum gases*, AVS Quantum Science **5**(4), 044401 (2023), doi:[10.1116/5.0163850](https://doi.org/10.1116/5.0163850).

[16] F. Fitzek, J.-N. Siemß, S. Seckmeyer, H. Ahlers, E. M. Rasel, K. Hammerer and N. Gaaloul, *Universal atom interferometer simulation of elastic scattering processes*, Scientific Reports **10**(1), 22120 (2020), doi:[10.1038/s41598-020-78859-1](https://doi.org/10.1038/s41598-020-78859-1).

[17] E. M. Stein and R. Shakarchi, *Fourier analysis: an introduction*, vol. 1, Princeton University Press (2003).

[18] L. Hörmander, *The analysis of linear partial differential operators. I. Classics in Mathematics*, Springer-Verlag, Berlin (2003).

[19] E. M. Stein and R. Shakarchi, *Real analysis: measure theory, integration, and hilbert spaces*, vol. 1, Princeton University Press (2005).

[20] L. N. Trefethen, *Spectral methods in MATLAB*, SIAM (2000).

[21] M. Pharr, W. Jakob and G. Humphreys, *Physically Based Rendering: From Theory to Implementation*, The MIT Press, Cambridge London, fourth edition edn., ISBN 978-0-262-04802-6 (2023).

[22] A. Oppenheim and R. Schafer, *Discrete-Time Signal Processing*, Pearson Deutschland, ISBN 9781292025728 (2013).

[23] M. Unser, *Sampling - 50 years after Shannon*, Proceedings of the IEEE **88**(4), 569 (2000), doi:[10.1109/5.843002](https://doi.org/10.1109/5.843002).

[24] A. Jerri, *The Shannon sampling theorem - Its various extensions and applications: A tutorial review*, Proceedings of the IEEE **65**(11), 1565 (1977), doi:[10.1109/PROC.1977.10771](https://doi.org/10.1109/PROC.1977.10771).

[25] J. Muga, J. Palao, B. Navarro and I. Egusquiza, *Complex absorbing potentials*, Physics Reports **395**(6), 357 (2004), doi:<https://doi.org/10.1016/j.physrep.2004.03.002>.

[26] *NumPy FFT Module*, <https://numpy.org/doc/2.2/reference/generated/numpy.fft.fft.html>, (accessed on 2025-04-06).

[27] W. H. Press, S. A. Teukolsky, W. T. Vetterling and B. P. Flannery, *Numerical Recipes. The Art of Scientific Computing.*, Cambridge: Cambridge University Press, 3rd ed. edn., ISBN 978-0-521-88068-8 (2007).

[28] J. G. Proakis and D. G. Manolakis, *Digital Signal Processing*, Pearson Prentice Hall, Upper Saddle River, N.J, 4th ed edn., ISBN 978-0-13-187374-2 (2007).

[29] A. Meurer, A. Reines, R. Gommers, Y.-L. L. Fang, J. Kirkham, M. Barber, S. Hoyer, A. Müller, S. Zha, S. Shanabrook *et al.*, *Python array API standard: Toward array interoperability in the scientific python ecosystem*, In *Proceedings of the 22nd Python in Science Conference*, pp. 8–17, doi:[10.25080/gerudo-f2bc6f59-001](https://doi.org/10.25080/gerudo-f2bc6f59-001) (2023).

[30] L. de Moura and N. Bjørner, *Z3: An Efficient SMT Solver*, In C. R. Ramakrishnan and J. Rehof, eds., *Tools and Algorithms for the Construction and Analysis of Systems*, pp. 337–340. Springer, Berlin, Heidelberg, ISBN 978-3-540-78800-3, doi:[10.1007/978-3-540-78800-3\\_24](https://doi.org/10.1007/978-3-540-78800-3_24) (2008).

[31] S. A. Brown, M. Folk, G. Goucher, R. Rew and P. F. Dubois, *Software for Portable Scientific Data Management*, *Computers in Physics* **7**(3), 304 (1993), doi:[10.1063/1.4823180](https://doi.org/10.1063/1.4823180).

[32] R. Rew and G. Davis, *NetCDF: An interface for scientific data access*, *IEEE Computer Graphics and Applications* **10**(4), 76 (1990), doi:[10.1109/38.56302](https://doi.org/10.1109/38.56302).

[33] S. Hoyer and J. Hamman, *Xarray: N-D labeled Arrays and Datasets in Python*, *Journal of Open Research Software* **5**(1), 10 (2017), doi:[10.5334/jors.148](https://doi.org/10.5334/jors.148).

[34] *FFTArray creation functions*, [https://qstheory.github.io/fftarray/v0.5.1/api/creation\\_functions\\_array.html](https://qstheory.github.io/fftarray/v0.5.1/api/creation_functions_array.html), (accessed on 2025-09-03) (2025).

[35] *Array API compatibility library*, <https://data-apis.org/array-api-compat/index.html>, (accessed on 2025-06-26), Version 1.12 (2025).

[36] P. Moin, *Fundamentals of Engineering Numerical Analysis*, Cambridge University Press, Cambridge, 2 edn., doi:[10.1017/CBO9780511781438](https://doi.org/10.1017/CBO9780511781438) (2010).

[37] Sunaina, M. Butola and K. Khare, *Calculating numerical derivatives using Fourier transform: Some pitfalls and how to avoid them*, *European Journal of Physics* **39**(6), 065806 (2018), doi:[10.1088/1361-6404/aadda6](https://doi.org/10.1088/1361-6404/aadda6).

[38] T. Jahnke and C. Lubich, *Error Bounds for Exponential Operator Splittings*, *BIT Numerical Mathematics* **40**(4), 735 (2000), doi:[10.1023/A:1022396519656](https://doi.org/10.1023/A:1022396519656).

[39] M. Thalhammer, *High-Order Exponential Operator Splitting Methods for Time-Dependent Schrödinger Equations*, *SIAM Journal on Numerical Analysis* **46**(4), 2022 (2008), doi:[10.1137/060674636](https://doi.org/10.1137/060674636).

[40] C. Neuhauser and M. Thalhammer, *On the convergence of splitting methods for linear evolutionary Schrödinger equations involving an unbounded potential*, *BIT Numerical Mathematics* **49**(1), 199 (2009), doi:[10.1007/s10543-009-0215-2](https://doi.org/10.1007/s10543-009-0215-2).

[41] E. Hansen and A. Ostermann, *Exponential splitting for unbounded operators*, *Mathematics of Computation* **78**(267), 1485 (2009), doi:[10.1090/S0025-5718-09-02213-3](https://doi.org/10.1090/S0025-5718-09-02213-3).

[42] E. Kieri, *Stiff convergence of force-gradient operator splitting methods*, Applied Numerical Mathematics **94**, 33 (2015), doi:[10.1016/j.apnum.2015.03.005](https://doi.org/10.1016/j.apnum.2015.03.005).

[43] D. An, D. Fang and L. Lin, *Time-dependent unbounded Hamiltonian simulation with vector norm scaling*, Quantum **5**, 459 (2021), doi:[10.22331/q-2021-05-26-459](https://doi.org/10.22331/q-2021-05-26-459).

[44] D. Burgarth, P. Facchi, A. Hahn, M. Johnsson and K. Yuasa, *Strong error bounds for Trotter and strang-splittings and their implications for quantum chemistry*, Physical Review Research **6**(4), 043155 (2024), doi:[10.1103/PhysRevResearch.6.043155](https://doi.org/10.1103/PhysRevResearch.6.043155).

[45] Matterwave library, <https://github.com/QSTheory/matterwave>, (accessed on 2025-09-03) (2025).

[46] P. R. Berman, *Atom Interferometry*, Elsevier, ISBN 978-0-12-092460-8, doi:[10.1016/B978-0-12-092460-8.X5000-0](https://doi.org/10.1016/B978-0-12-092460-8.X5000-0) (1997).

[47] G. M. Tino and M. A. Kasevich, eds., *Atom Interferometry: Proceedings of the International School of Physics "Enrico Fermi"*, Course 188, Varenna on Lake Como, Villa Monastero, 15 - 20 July 2013, IOS Press, Amsterdam, ISBN 978-1-61499-448-0 978-1-61499-447-3 978-88-7438-087-9 (2014).

[48] H. Müller, S.-w. Chiow, Q. Long, S. Herrmann and S. Chu, *Atom Interferometry with up to 24-Photon-Momentum-Transfer Beam Splitters*, Physical Review Letters **100**(18), 180405 (2008), doi:[10.1103/PhysRevLett.100.180405](https://doi.org/10.1103/PhysRevLett.100.180405).

[49] S.-w. Chiow, T. Kovachy, H.-C. Chien and M. A. Kasevich, *102 $\hbar k$  Large Area Atom Interferometers*, Physical Review Letters **107**(13), 130403 (2011), doi:[10.1103/PhysRevLett.107.130403](https://doi.org/10.1103/PhysRevLett.107.130403).

[50] H. Ahlers, H. Müntinga, A. Wenzlawski, M. Krutzik, G. Tackmann, S. Abend, N. Gaaloul, E. Giese, A. Roura, R. Kuhl, C. Lämmerzahl, A. Peters *et al.*, *Double Bragg Interferometry*, Physical Review Letters **116**(17), 173601 (2016), doi:[10.1103/PhysRevLett.116.173601](https://doi.org/10.1103/PhysRevLett.116.173601).

[51] M. Gebbe, J.-N. Siemß, M. Gersemann, H. Müntinga, S. Herrmann, C. Lämmerzahl, H. Ahlers, N. Gaaloul, C. Schubert, K. Hammerer, S. Abend and E. M. Rasel, *Twin-lattice atom interferometry*, Nature Communications **12**(1), 2544 (2021), doi:[10.1038/s41467-021-22823-8](https://doi.org/10.1038/s41467-021-22823-8).

[52] P. Meystre, *Atom Optics*, vol. 33, Springer Science & Business Media, ISBN 978-1-4419-2930-3 978-1-4757-3526-0, doi:[10.1007/978-1-4757-3526-0](https://doi.org/10.1007/978-1-4757-3526-0) (2001).

[53] G. Grynberg, A. Aspect, C. Fabre and C. Cohen-Tannoudji, *Introduction to Quantum Optics: From the Semi-classical Approach to Quantized Light*, Cambridge University Press, 1 edn., ISBN 978-0-521-55112-0 978-0-521-55914-0 978-0-511-77826-1, doi:[10.1017/CBO9780511778261](https://doi.org/10.1017/CBO9780511778261) (2010).

[54] D. A. Steck, *Rubidium 87 D Line Data*, <http://steck.us/alkalidata>, (revision 2.3.3, 28 May 2024).

[55] NVIDIA ADA GPU ARCHITECTURE, <https://images.nvidia.com/aem-dam/Solutions/ geforce/ada/nvidia-ada-gpu-architecture.pdf>, (accessed on 2024-05-16).

[56] H. Ahlers, L. Badurina, A. Bassi, B. Battelier, Q. Beaufils, K. Bongs, P. Bouyer, C. Braxmaier, O. Buchmueller, M. Carlesso, E. Charron, M. L. Chiofalo *et al.*, *STE-QUEST: Space Time Explorer and QUantum Equivalence principle Space Test*, doi:[10.48550/arXiv.2211.15412](https://doi.org/10.48550/arXiv.2211.15412) (2022), [2211.15412](https://arxiv.org/abs/2211.15412).

[57] C. Struckmann, R. Corgier, S. Loriani, G. Kleinsteinberg, N. Gox, E. Giese, G. Métris, N. Gaaloul and P. Wolf, *Platform and environment requirements of a satellite quantum test of the weak equivalence principle at the  $10^{-17}$  level*, Physical Review D **109**(6), 064010 (2024), doi:[10.1103/PhysRevD.109.064010](https://doi.org/10.1103/PhysRevD.109.064010).

[58] R. Corgier, S. Loriani, H. Ahlers, K. Posso-Trujillo, C. Schubert, E. M. Rasel, E. Charron and N. Gaaloul, *Interacting quantum mixtures for precision atom interferometry*, New Journal of Physics **22**(12), 123008 (2020), doi:[10.1088/1367-2630/abcbc8](https://doi.org/10.1088/1367-2630/abcbc8).

[59] *FFTArray dual-species ground state example*, [https://github.com/QSTheory/fftarray/blob/v0.5.1/examples/two\\_species\\_groundstate.ipynb](https://github.com/QSTheory/fftarray/blob/v0.5.1/examples/two_species_groundstate.ipynb), (accessed on 2025-09-03) (2025).

[60] *JAX: Structured control flow primitives*, <https://docs.jax.dev/en/latest/control-flow.html#structured-control-flow-primitives>, (accessed on 2025-05-19).

[61] *TorchGPE Documentation - The Gas Class*, [https://qo-eth.github.io/TorchGPE/user\\_guide/fundamentals.gas\\_class.html](https://qo-eth.github.io/TorchGPE/user_guide/fundamentals.gas_class.html), (accessed on 2025-06-26).

[62] R. Li, V. J. Martínez-Lahuerta, S. Seckmeyer, K. Hammerer and N. Gaaloul, *Robust double Bragg diffraction via detuning control*, Physical Review Research **6**(4), 043236 (2024), doi:[10.1103/PhysRevResearch.6.043236](https://doi.org/10.1103/PhysRevResearch.6.043236).

[63] J. Lecoffre, A. Hadi, M. Bruneau, C. Garcion, N. Fabre, É. Charron, N. Gaaloul, G. Dutier and Q. Bouton, *Measurement of Casimir-Polder interaction for slow atoms through a material grating*, Physical Review Research **7**(1), 013232 (2025), doi:[10.1103/PhysRevResearch.7.013232](https://doi.org/10.1103/PhysRevResearch.7.013232).

[64] K. Frye-Arndt, M. Glaysher, M. Glaeser, M. Koch, S. Seckmeyer, H. Ahlers, W. Herr, N. Gaaloul, C. Schubert and E. Rasel, *Large, ultra-flat optical traps for uniform quantum gases*, doi:[10.48550/ARXIV2505.14155](https://arxiv.org/abs/2505.14155) (2025).

[65] M. Bruneau, J. Lecoffre, G. Routier, N. Gaaloul, G. Dutier, Q. Bouton and T. Emig, *Probing the geometry dependence of the Casimir-Polder interaction by matter-wave diffraction at a nano-grating*, doi:[10.48550/ARXIV.2505.10056](https://arxiv.org/abs/2505.10056) (2025).

[66] *NVIDIA A100 | Tensor Core GPU*, <https://www.nvidia.com/content/dam/en-zz/Solutions/Data-Center/a100/pdf/nvidia-a100-datasheet-nvidia-us-2188504-web.pdf>, (accessed on 2024-05-16).